

Modeling and Simulation of an Active Hydraulic Heave Compensation System for Offshore Cranes

Jørgen Sverdrup-Thygeson

Master of Science in Engineering Cybernetics

Submission date: June 2007

Supervisor: Olav Egeland, ITK

Co-supervisor: Jan Tommy Gravdahl, ITK

Tristan Perez, Centre for Ships and Ocean Structures
(CeSOS)

Problem Description

Offshore cranes can be equipped with active hydraulic heave compensators in combination with pneumatic accumulators for passive heave compensation. In this study a dynamic model is to be developed for this type of heave compensator. This includes models for hydraulics, pneumatics, cable dynamics and vessel response to waves.

1. Present existing systems for heave compensation of cranes.
2. Discuss dynamic models for active hydraulic heave compensators with passive pneumatic damping using the bond graph formalism.
3. Develop a mathematical model for an active hydraulic heave compensator with passive pneumatic damping.
4. Implement the dynamic model in Simulink and study the performance of the heave compensator under relevant wave conditions.

Assignment given: 08. January 2007
Supervisor: Olav Egeland, ITK

Abstract

This thesis deals with the mathematical modeling of hydraulic heave compensation systems. When performing operations such as launch and recovery of remote operated vehicles and lowering subsea installation parts to the sea floor, it is important to attenuate unwanted load motion caused by elongation of the cable and heave motion of the vessel. Quite often, such operations must be put off while waiting for the weather to calm down. Extending the window of operations by developing equipment that can handle varying sea states can result in significant cost savings.

There exist both electric and hydraulic heave compensation devices, but the main focus of this thesis is on the hydraulic configurations. A mathematical model is developed in Simulink, and simulations are performed for long-crested seas with values corresponding to the average sea conditions in the North Sea.

Acknowledgements

I would like to thank my supervisor Professor Olav Egeland at the Department of Engineering Cybernetics for introducing me to hydraulic systems. Thanks also to my co-advisor Dr. Tristan Perez for helpful insight into the topic of heave compensation and for great help on theoretical aspects concerning characterization of vessel motion.

Trondheim, June 4, 2007

Jørgen Sverdrup-Thygeson

Contents

Abstract	i
Acknowledgements	iii
1 Introduction	1
1.1 Motivation	1
1.2 Problem statement	2
1.3 Report organization and main contribution	2
2 Description of ocean waves	3
3 Characterization of vessel motion due to incident waves	6
3.1 Environmental forces	7
3.2 Force to motion frequency response	8
3.3 Calculating vessel motion time-series	9
4 Different kinds of heave compensators	10
4.1 Nodding boom	11
4.2 Hydraulic flying sheave	12
4.3 Electric winch drum	14
4.4 Sub A-frame	14
5 Bond graph theory	16
5.1 Bond graph components	16
5.1.1 Bonds and bond graph variables	17
5.1.2 Passive 1-ports	17
5.1.3 Active 1-ports	18
5.1.4 Junctions	18
5.1.5 2-port elements	19
5.2 Assignment of causality	19
5.3 Converting bond graphs into block diagrams	21

6	Modeling of the heave compensator system	23
6.1	Modeling of the cable	26
6.2	Equations of motion for the load	27
6.3	Equations of motion for the sheave	27
6.4	Passive heave compensation	28
6.5	Active heave compensation	33
6.5.1	Static dimensioning	33
6.5.2	Transfer function and control law	35
6.6	Performance in regular waves	39
6.7	Performance in irregular waves	41
6.8	Undesirable scenarios	46
6.8.1	Resonance	46
6.8.2	Loss of supply pressure	50
6.9	Control loop for a pump with variable displacement	52
7	Conclusion and further work	55
7.1	Conclusion	55
7.2	Suggestions for further work	55
A	Simulink diagrams	59

Chapter 1

Introduction

1.1 Motivation

The sea conditions offshore can be rather harsh, and quite often critical operations must be put off until the weather calms down. Extending the window of operations by developing equipment that can handle varying sea states can result in significant cost savings. Dynamic positioning systems have been developed to keep vessels steady in the horizontal plane by using thrusters, but the vertical motion of the vessel can still be large. The magnitude of the heave motion can be several meters, depending on the sea state. Operations such as launch and recovery of remote operated vehicles (ROVs) and lowering subsea installation parts to the seabed are especially vulnerable. It would be advantageous, and often safety critical, to be able to keep the load still. A heave compensation device enables this to be done. As the name suggests, this device is used to counteract the heave of the vessel. The motion of the vessel is measured, and the heave compensator provides reciprocal attenuation of this motion. To the author's knowledge, present heave compensation systems can operate with depths of up to 2500 meters and load mass up to 350 tonnes.

1.2 Problem statement

Hydraulic heave compensation systems consist of many different components, each with its own dynamics. Together, they make up a fairly complex system, and it is invaluable to be able to simulate the behavior of the system and identify possible failures before it is put to use. It is also important to evaluate the performance under different working conditions. The problem statement of this thesis can be formulated as follows:

"How can a mathematical model of a hydraulic heave compensation system be implemented in Simulink, and what is the attainable performance of such a system?"

1.3 Report organization and main contribution

Swell and wind generated waves are the sources of the heave motion of the vessel. Only the latter is considered in this thesis. Ocean waves are random, and a stochastic approach to the characterization of the sea spectrum is presented in chapter 2. How the wave amplitudes are converted into vessel heave is further explained in chapter 3. Response amplitude operators, or RAOs, are a key concept here.

There are essentially two types of heave compensation devices, electrical and hydraulic. Hydraulic compensators are the main topic of this thesis, but a summary of advantages and disadvantages of different configurations is given in chapter 4.

Hydraulic heave compensators are complex systems with a lot of components. Developing a mathematical model complete with all physical effects is a time-consuming task. The first part of chapter 6 presents a model which includes the most significant effects. The main contribution of this thesis is the development of a Simulink model of a hydraulic heave compensator. Appendix A contains the block diagrams. Chapter 5 presents a summary of the bond graph theory and explains how this is used to create the Simulink model. Simulations for both regular and irregular seas are performed and presented in sections 6.6 and 6.7. Two scenarios the developers of heave compensation devices should keep in mind are described in section 6.8.

Chapter 2

Description of ocean waves

The elevation of the sea surface for regular waves in deep water is given by (Perez, 2005a)

$$\zeta(x, y, t) = \bar{\zeta} \sin [\omega t + \epsilon - kx \cos(\chi) - ky \sin(\chi)] \quad (2.1)$$

where $\omega = \frac{2\pi}{T}$ is the wave frequency, $k = \frac{\omega^2}{g}$ is the wave number, ϵ is the phase of the wave and χ is the encounter angle.

The random nature of ocean waves prevents them from being accurately represented by a single sinusoidal wave. A stochastic approach is therefore necessary. It is assumed that the statistics of the random process varies much more slowly than the realization itself. The stochastic process of the ocean waves can thus be considered stationary. This assumption is valid for low and moderate seas with significant wave height¹ below 4 meters (Perez, 2005a). The process is also assumed to be Gaussian with zero mean, and this yields the following statistics

$$\mathbf{E}[\zeta(t)] = 0, \text{ var}[\zeta] = \mathbf{E}[\zeta(t)^2] = \int_0^\infty \mathbf{S}_{\zeta\zeta}(\omega) d\omega \quad (2.2)$$

where $\mathbf{S}_{\zeta\zeta}$ is the power spectral density (PSD) of the sea surface elevation. The spectral moments of the stochastic process are important, and they are defined as

$$m_\zeta^n = \int_0^\infty \omega^n \mathbf{S}_{\zeta\zeta}(\omega) d\omega \quad (2.3)$$

If wave measurements are available for the desired location, these can be used to form the correct power spectral density function. The significant wave height, $H_{1/3}$, and the average wave period, \bar{T} , can then be estimated by

¹Average of the highest one third of the waves

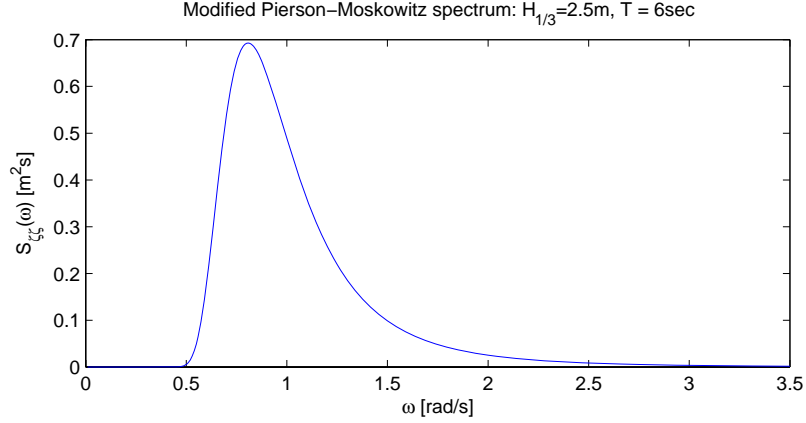


Figure 2.1: Standard wave spectrum for the North Sea with no swell

$$\bar{T} = 2\pi \frac{m_{\zeta}^0}{m_{\zeta}^1} \quad (2.4)$$

$$H_{1/3} = 4\sqrt{m_{\zeta}^0} \quad (2.5)$$

Standard, idealized spectra can be used if measurements are not obtainable. The recommendation from the ITTC² is the Modified Pierson-Moskowitz (MPM), or ISSC³, spectra given by (ISSC, 1964)

$$\mathbf{S}_{\zeta\zeta}(\omega) = \frac{A}{\omega^5} e^{\frac{-B}{\omega^4}} \quad (2.6)$$

where

$$A = \frac{172.53H_{1/3}^2}{\bar{T}^4}, \quad B = \frac{689.97}{\bar{T}^4} \quad (2.7)$$

The Modified Pierson-Moskowitz spectra are valid for fully developed seas with no swell and unlimited fetch. Limited fetch is accounted for in the JONSWAP spectra, while the effect of swell is considered in the double-peak Torsethaugen spectra (Perez, 2005a). The modal frequency of the MPM spectra is given by

$$\omega_0 = \left(\frac{4B}{5}\right)^{1/4} \quad (2.8)$$

²International Towing Tank Conference

³International Ship and Offshore Structures Congress

Realizations of the sea surface elevation for irregular seas can be approximated by (Perez, 2005a)

$$\zeta(t) = \sum_{n=1}^N \bar{\zeta}_n \cos(\omega_n t + \epsilon_n) \quad (2.9)$$

Irregular waves can thus be represented by a sum of several regular waves (see Equation (2.1)) with different amplitude, frequency and phase. There are two kinds of irregular waves, long-crested and short-crested. The type of waves considered in this thesis is long-crested, even though ocean waves are most likely to be short-crested. Long-crested waves means that the wave crests are assumed to be parallel and moving in the same direction, the direction of the dominant wind component. For more accurate simulations of ship motions it is important to also account for the energy in the waves that strike the vessel at other angles than the dominant encounter angle (Perez, 2005a). The simplifying assumption of long-crested seas can be justified because the ship motions are not the main topic of this thesis. For long-crested seas, $\bar{\zeta}_n$ can be calculated by (Perez, 2005a)

$$\bar{\zeta}_n = \sqrt{2\mathbf{S}_{\zeta\zeta}(\omega^*)\Delta\omega} \quad (2.10)$$

where ω^* is selected randomly in

$$\omega^* \in \left[\omega_n - \frac{\Delta\omega}{2}, \omega_n + \frac{\Delta\omega}{2} \right]$$

Combining Equations (2.9) and (2.10) and substituting ω^* for ω_n then yields

$$\zeta(t) = \sum_{n=1}^N \sqrt{2\mathbf{S}_{\zeta\zeta}(\omega^*)\Delta\omega} \cos(\omega^* t + \epsilon_n) \quad (2.11)$$

If the sea surface elevation is to be calculated at more than one spacial coordinate, the encounter angle must be accounted for as shown in Equation (2.12).

$$\zeta(x, y, t) = \sum_{n=1}^N \sqrt{2\mathbf{S}_{\zeta\zeta}(\omega^*)\Delta\omega} \cos(\omega^* t + \epsilon_n - k_n(x \cos \chi - y \sin \chi)) \quad (2.12)$$

The time-series of the waves used for simulations in this thesis are calculated using a significant wave height of 2,5 meters and an average wave period of 6 seconds. According to the wave climate atlas at <http://www.oceanweather.net/MS50WaveAtlas/> these values are appropriate for the North Sea Basin. The atlas is based on results from the MSC50 study described in Swail *et al.* (2006). Recent and historical data for some other locations are available at <http://www.ndbc.noaa.gov/>.

Chapter 3

Characterization of vessel motion due to incident waves

The motion of the vessel in the hydrodynamic frame, or h-frame, due to incident waves is described in this chapter. This is referred to in literature as a seakeeping model. The horizontal axes of the h-frame coincide with the mean free surface of the ocean, with one axis pointing forward, aligned with the low-frequency heading angle $\bar{\psi}^1$. The other axis points starboard and the third axis points downward. It is important to note that the hydrodynamic frame is not fixed to the hull, but rather follows the path of the hull at the average speed of the vessel (Perez, 2005*b*). The low-frequency motion is considered small as the vessel is assumed to be operating in DP². The most important assumptions for modeling are:

- The velocity of the vessel is close to zero.
- The h-frame can be considered inertial.
- The load being deployed does not affect the motion of the vessel significantly.

The second assumption leads to the vector equation of motion given in Equation (3.1) (Perez, 2005*a*).

$$\mathbf{M}_{RB}^h \ddot{\boldsymbol{\xi}} = \boldsymbol{\tau}_{hyd}^h \quad (3.1)$$

The coordinates $\boldsymbol{\xi}$ are generalised perturbation coordinates. When the vessel is undisturbed, the origin of the h-frame coincides with a point s on the vessel. The perturbation of this point from its equilibrium position is represented by

¹The heading angle when the first-order wave-induced motion is filtered out.

²This means that the low-frequency heading angle $\bar{\psi}$ is nearly constant.

the surge, sway and heave perturbations, ξ_1 , ξ_2 , and ξ_3 , respectively. Usually, the s-axes are considered parallel to the body frame (b-frame) axes given by the principal axes of inertia. This means that the perturbation angles $[\xi_4, \xi_5, \xi_6]^T$ are the Euler angles between the h-frame and the b-frame. For the application studied in this thesis, only the heave motion is considered.

The hydrodynamic force vector $\boldsymbol{\tau}_{hyd}$ is composed of the following components

$$\boldsymbol{\tau}_{hyd} = \boldsymbol{\tau}_{1w} + \boldsymbol{\tau}_{2w} + \boldsymbol{\tau}_r + \boldsymbol{\tau}_v + \boldsymbol{\tau}_{hs}, \quad (3.2)$$

where $\boldsymbol{\tau}_{1w}$ and $\boldsymbol{\tau}_{2w}$ are first-order (oscillatory) and second-order (non-oscillatory) wave excitation forces, respectively, $\boldsymbol{\tau}_r$ are radiation induced forces, $\boldsymbol{\tau}_v$ are viscous damping forces, and $\boldsymbol{\tau}_{hs}$ are hydrostatic forces, also called restoring forces, due to gravity and buoyancy.

3.1 Environmental forces

Environmental forces include forces and moments caused by wind, current, and waves ($\boldsymbol{\tau}_{1w} + \boldsymbol{\tau}_{2w}$). Only the latter is considered in this thesis. Wave forces can be split into first-order and second-order wave excitation forces. The second-order forces are assumed to be compensated by the positioning system. Therefore, they are not considered in the model. First-order wave excitation forces are composed of Froude-Kryloff and diffraction forces. According to Faltinsen (1990) these forces can be explained as follows

Froude-Kryloff forces Forces due to the incident waves under the assumption that the hull is restrained from moving and that the presence of the hull does not disturb the flow field

Diffraction forces A correction to account for the modification of the flow field due to the hull

The vessel lines of a scaled supply vessel model are imported into the program ShipX VERES (Fathi, 2004) and used to calculate the so-called Force Response Amplitude Operators (FRAOs). FRAOs are essentially frequency response functions that map sinusoidal wave amplitudes into forces on the hull. By assuming linearity and combining the wave spectrum from chapter 2 with the FRAOs, the spectrum for the first-order wave excitation forces is obtained:

$$\mathbf{S}_{\tau_{1w}\tau_{1w}i}(\omega) = |F_i(j\omega)|^2 \mathbf{S}_{\zeta\zeta}(\omega), \quad i = 1, 2, \dots, 6 \quad (3.3)$$

3.2 Force to motion frequency response

The radiation induced forces and moments, $\boldsymbol{\tau}_r$, can be expressed by

$$\boldsymbol{\tau}_r^h = -\mathbf{A}^h(\omega)\ddot{\boldsymbol{\xi}} - \mathbf{B}^h(\omega)\dot{\boldsymbol{\xi}}. \quad (3.4)$$

Equation (3.4) shows that the radiation induced forces consist of two components, which are proportional to the perturbation acceleration and velocity, respectively (Faltinsen, 1990). The first component is due to added mass, which can be explained as (Perez, 2005a) forces that "reflect the change of momentum in the fluid due to the motion of the hull." The second component accounts for the potential damping, which is energy dissipation due to generated waves. Both the added mass and the potential damping matrices are calculated by VERES.

Hydrostatic forces and moments are proportional to the perturbations $\boldsymbol{\xi}$ and can be expressed in a linear form by (Perez, 2005a)

$$\boldsymbol{\tau}_{hs}^h = \mathbf{G}^h \boldsymbol{\xi} \quad (3.5)$$

Combining Equations (3.1), (3.2), (3.4) and (3.5) and considering sinusoidal motion:

$$\left[\mathbf{M}_{RB}^h + \mathbf{A}^h(\omega) \right] \ddot{\boldsymbol{\xi}} + \mathbf{B}^h(\omega) \dot{\boldsymbol{\xi}} + \mathbf{G}^h \boldsymbol{\xi} = \boldsymbol{\tau}_{1w}^h \quad (3.6)$$

The potential damping is considered enough for heave motion. Equation (3.6) can also be considered in the frequency domain by (Perez and Lande, 2006)

$$\left[-\omega^2(\mathbf{M}_{RB}^h + \mathbf{A}^h(\omega)) + j\omega\mathbf{B}^h(\omega) + \mathbf{G}^h \right] \tilde{\boldsymbol{\xi}}(j\omega) = \tilde{\boldsymbol{\tau}}_{1w}^h(j\omega) \quad (3.7)$$

where $\tilde{\boldsymbol{\xi}}$ and $\tilde{\boldsymbol{\tau}}_{1w}^h$ are complex operators. The force to motion frequency response for the first-order wave excitation forces can then be written

$$\mathbf{G}_d(j\omega) = \left[-\omega^2(\mathbf{M}_{RB}^h + \mathbf{A}^h(\omega)) + j\omega\mathbf{B}^h(\omega) + \mathbf{G}^h \right]^{-1} \quad (3.8)$$

Multiplying the force RAOs and the force to motion frequency response yields what is called motion RAOs (MRAOs). This is expressed as

$$\mathbf{H}(j\omega) = \mathbf{G}_d(j\omega)\mathbf{F}(j\omega) \quad (3.9)$$

The spectrum for the vessel motion is then obtained as in Equation (3.3)

$$\mathbf{S}_{\xi\xi,i}(\omega) = |H_i(j\omega)|^2 \mathbf{S}_{\zeta\zeta}(\omega), \quad i = 1, 2, \dots, 6 \quad (3.10)$$

Figure 3.1 shows the wave spectrum compared to the heave motion spectrum.

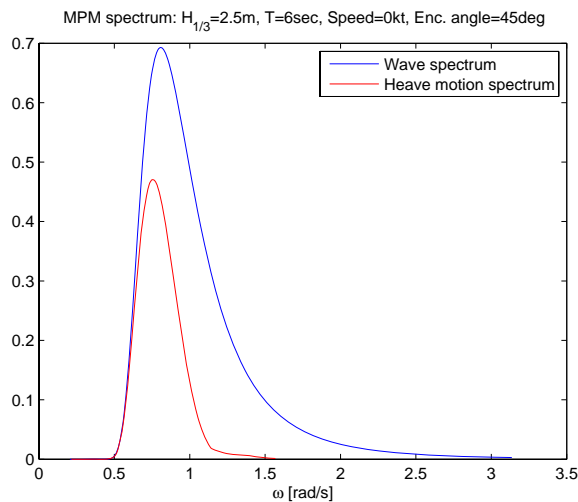


Figure 3.1: Wave spectrum and heave motion spectrum

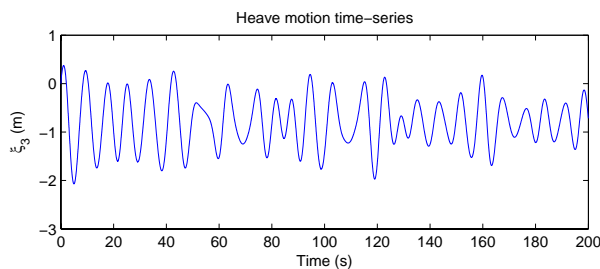


Figure 3.2: Time-series of vessel heave motion

3.3 Calculating vessel motion time-series

In the same way as in Equation (2.11), a realization of the vessel motion in the time domain can be calculated using the motion spectrum from Equation (3.10).

$$\xi_i(t) = \sum_{n=1}^N \sqrt{2S_{\xi\xi,i}(\omega^*)\Delta\omega} \cos(\omega^*t + \arg[H_i(j\omega)] + \epsilon_n) \quad (3.11)$$

The time-series of the heave motion of the vessel is shown in figure 3.2.

Chapter 4

Different kinds of heave compensators

Vertical motion attenuation can be achieved in several ways. Adamson (2003) explains four different methods:

- Nodding boom
- Hydraulic flying sheave
- Electric winch drum
- Sub A-frame

Before going into more details about each configuration, it is important to clarify the difference between passive and active heave compensation. Passive heave compensators contain no sources of energy. They simply absorb energy created by the motion of the vessel and store this as some form of potential energy. The passive system can be thought of as a spring-damper with a fairly soft spring. Heave compensation devices are often designed with an integrated passive system which is operational even if the active system fails. To ensure stability of the closed-loop heave compensation system it is important that there is some form of natural damping in the load path. Viscous drag on the load and the cable provide some damping, but additional damping is also present within the passive system itself. In hydraulic cylinders, damping occurs due to viscous friction on the piston and leakage between the two chambers. Introducing a passive system which works as a soft spring into the load path has the disadvantage that it creates a new natural frequency in the overall system. Theoretically, this can cause resonance if the wave frequency matches the natural frequency of the passive compensator.

Active heave compensators contain devices that supply energy in order to keep the load close to its desired position. Sensors are mounted either on the

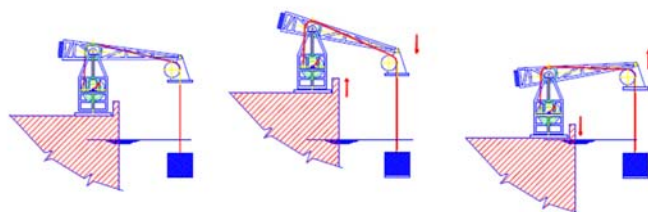


Figure 4.1: Nodding boom configuration. Illustration: Adamson (2003)

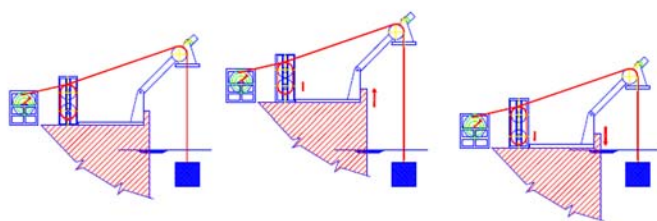


Figure 4.2: Hydraulic flying sheave configuration. Illustration: Adamson (2003)

vessel, the overboard crane or the load, and the inputs are used to actively control the motion of the heave compensator. Load cells, accelerometers, depth sounders and altitude sonars are the most common types of sensors. (Adamson, 2003)

When it comes to the cable laying there are generally two configurations that are being used. The first is when a sheave is mounted at the end of a crane that extends overboard and the cable is routed over this sheave. The A-frame configuration shown in figure 4.5 is the other.

4.1 Nodding boom

The nodding boom, also referred to as a heave compensated crane, consists of a sheave mounted at the end of a boom, as shown in figure 4.1. Moving the boom up and down compensates for the vessel motion. The winch is not used as a compensating device. Wear and tear on the cable is minimal as it does not move back and forth over the sheaves when the boom is moving. The primary lifting device, i.e., the winch is not prevented from working if the compensation system fails. The main disadvantages of the nodding boom configuration are the high inertia of the crane and the high power requirements to move it.

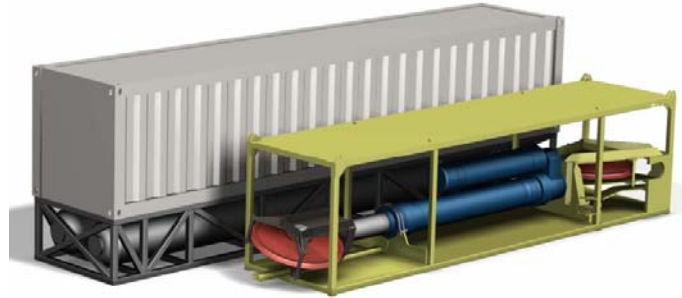


Figure 4.3: Active heave compensator from Gusto MSC. Illustration: GustoMSC (n.d.)



Figure 4.4: M/V "Normand Progress". Photo: Specification sheet by Solstad Shipping AS

4.2 Hydraulic flying sheave

In the flying sheave configuration the cable bends over two sheaves, and the compensating motion is achieved by controlling the separation between the sheaves. Changing the distance is usually accomplished with hydraulic cylinders. Due to the motion and the continuous bending of the cable over the sheaves, wear and tear can be a problem. The inherent problems of the nodding boom configuration are avoided because the inertia is much lower.

The multipurpose vessel M/V "Normand Progress" operated by Solstad Shipping AS was in 2003 equipped with a hydraulic heave compensator from Gusto MSC (see figure 4.3). As shown in figure 4.4, the vessel has an A-frame mounted at the stern. Figure 4.5 shows how the heave compensation device was installed between the winch and the A-frame.

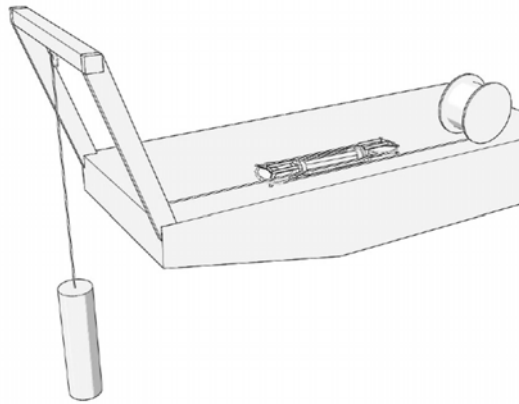


Figure 4.5: Hydraulic heave compensator in A-frame configuration. Illustration: Frumau and Woldering (2007)

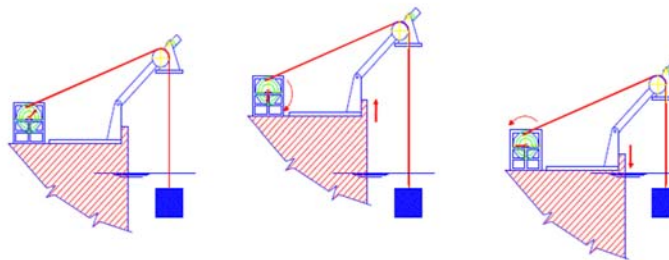


Figure 4.6: Electric winch drum configuration. Illustration: Adamson (2003)

4.3 Electric winch drum

The electric winch drum solution works by controlling the winch directly. Cable is alternately reeved in and payed out in response to the heave motion of the vessel. This means that the winch drum and all the remaining cable have to rotate back and forth. High inertia and power requirements are therefore a problem. The winch itself is the source of the compensating motion, and the life expectancy of the lifting device is thus shorter than for heave compensation systems which do not involve the winch. Some advantages of electric winch systems are (Drevdal, n.d.; Adamson, 2003):

- Require less space than traditional hydraulic systems
- Fewer moving parts reduce the vulnerability
- Can be retrofitted on existing winch systems
- Unlimited range of response
- Faster launch and recovery speeds than hydraulic systems

The most notable disadvantage is the large power requirements due to the high inertia of the winch drum and the cable. This problem can however be remedied by introducing regenerative techniques. Some energy can be stored while lowering the load and reused at a later time.

Despite all the advantages, electrical heave compensators are still outnumbered by the hydraulic configurations. The reason is partly because the first AC driven drawworks was not delivered until 1995 (Offshore, 1999). An electric winch system can be used with both the overboard crane and the A-frame configurations.

4.4 Sub A-frame

The sub A-frame configuration is a fairly new invention that was patented in 2000¹. It is similar to the nodding boom, but the size, complexity and inertia are much lower. The configuration consists of a smaller A-frame connected to an existing full-size A-frame, pivoting at the bottom and connected by lifting wires at the top. Some kind of active or passive heave compensation devices, either winches or hydraulic cylinders, are used to control the motion of the lifting wires in response to the vessel motion. Redundancy of these elements is of utmost importance. The sub A-frame solution exploits advantages from both the nodding boom and the flying sheave concept, by being kind to the cable and at the same time have a low inertia. Figure 4.8 shows how the system can be set up with winches as auxiliary lifting devices.

¹<http://www.patentstorm.us/patents/6082947-description.html>

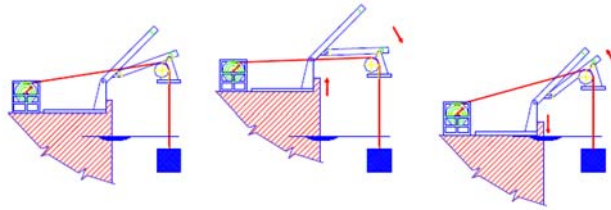


Figure 4.7: Sub A-frame configuration. Illustration: Adamson (2003)

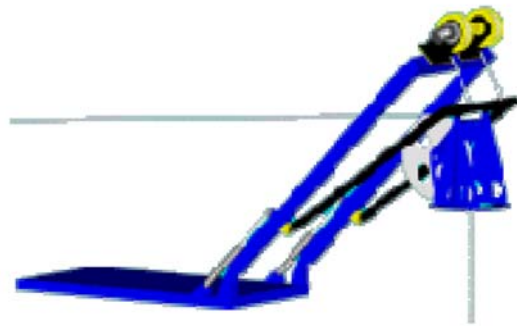


Figure 4.8: Sub A-frame configuration with auxiliary winches. Illustration: Adamson (2003)

Chapter 5

Bond graph theory

Mathematical models come in many forms, and not all of them contain equations. In fact, most of them rely on some sort of graphical representation instead. A reason for this is that the equations themselves are often so complex that they yield very limited insight into the dynamic behavior. Representing system variables as signals flowing between blocks that perform certain mathematical operations may lead to a better understanding of the system. This type of model is called a block diagram and is recognized as the idea behind Simulink models. However, it is not always a simple task to choose which physical signals to use as system variables. Typically, in control engineering, the states of the system components are selected, because it yields good insight into the physics of the system. Not surprisingly, this is referred to as the state-variable form. Another type of model that relies on state variables is the bond graph, which is the topic of this section.

A bond graph is an abstract mathematical model which implicitly contains a lot of information. The term bond graph was invented by H. M. Paynter in the late 1950s. One of the most important advantages of bond graphs is that the same symbols are used to represent a wide range of different physical systems, such as mechanical, electrical, thermal, and hydraulic systems, as well as combinations of these (Rosenberg and Karnopp, 1983). For an extensive review of bond graph theory, the reader is referred to Pedersen and Engja (2003) and Rosenberg and Karnopp (1983). The summary presented in this chapter is mostly based on theory from Rosenberg and Karnopp (1983).

5.1 Bond graph components

Bond graphs consist in general of five types of components, active and passive 1-ports, 2-port elements, junctions, and of course, bonds. Each of these are explained in more detail below.

Table 5.1: Bond graph variables. Adapted from Pedersen and Engja (2003)

Energy domain	Effort (e)	Flow (f)	Momentum (p)	Displacement (q)
Electrical	Voltage [V]	Current [A]	Flux linkage [Vs]	Charge [As] or [C]
Mechanical translation	Force [N]	Velocity [m/s]	Linear momentum [kgm/s]	Distance [m]
Mechanical rotation	Torque [Nm]	Angular velocity [rad/s]	Angular momentum [Nms]	Angle [rad]
Hydraulic	Pressure [Pa]	Volume flow rate [m^3/s]	Pressure momentum [N/m^2s]	Volume [m^3]
Thermal	Temperature [K]	Entropy flow [J/s]	(not defined)	Entropy [J]

5.1.1 Bonds and bond graph variables

A bond is basically a line that connects two parts of a system. Associated with this line are two signals with opposite directions. One is called *effort* and the other *flow*, and they are denoted e and f respectively. A fundamental idea behind bond graph theory is that the product of these two signals is power. Therefore, the bonds indicate that power is flowing between the model components. The power variables effort and flow are generalized variables with different meanings depending on the type of system being modeled. For a translational mechanical system effort is a force applied to a system component, while flow is the velocity of this component. As power is the time derivative of energy, the power variables are always the time derivatives of the variables that describe the energy of a system. The associated generalized energy variables are called the *momentum*, p , and the *displacement*, q . The four generalized variables are the only variables that are used in bond graphs. Table 5.1 shows how the power and energy variables are selected for different kinds of systems.

The bonds are actually not just lines, they are half arrows, and the arrows indicate the direction of positive power flow, that is, when both effort and flow have the same sign.

5.1.2 Passive 1-ports

These elements are called 1-ports, because they are only connected to one bond, and passive because they do not contain any power sources. There are three types of 1-ports, namely resistor, capacitor, and inertia elements. They are not specifically related to electrical systems, although the names suggest it. The mathematical relations for linear 1-ports are shown in table

Table 5.2: Mathematical relations for linear 1-ports

Resistor	$e = Rf$
Capacitor	$e = \frac{1}{C}q = \frac{1}{C} \int f$
Inertia	$f = \frac{1}{I}p = \frac{1}{I} \int e$

5.2, but the relations can often be nonlinear.

The resistor element, R, relates flow directly to the effort and is representative of frictional losses. Friction dissipates power, and therefore the half arrow always points towards the resistor element.

A capacitor, C, relates displacement, or the time integral of flow, to effort. For translational mechanical systems flow is the velocity and hence, displacement will be position. A mechanical spring relates force to the deflection of the spring and can thus be represented by a capacitor element. In hydraulic systems, a capacitor is representative of a hydraulic volume and relates the time integral of flow rate to pressure, according to table 5.1. Capacitors are elements that store and release energy. They are ideal elements in the sense that no energy is lost and thus, capacitors are energy conservative. Since power flow is actually the rate of energy storage, it is illustrative to point the half arrow towards the C.

Inertia elements, I, relate momentum to flow. They are energy storage elements and energy conservative, just like the capacitors. The half arrow points towards the element for the same reason as above. Mass, rotational inertia and fluid inertia are examples of physical effects that can be represented by an inertia element.

5.1.3 Active 1-ports

Active 1-ports are called active because they contain sources of power. There are two types of active 1-ports, effort sources and flow sources. They are ideal elements in the sense that the effort source is not influenced by the flow coming in the other direction, and the opposite for the flow source. An example of an effort source is the force of gravity. The flow source can be a source of for instance velocity or flow rate. Usually, the half arrows point away from the source to show that the source is an active element that delivers power to the passive elements.

5.1.4 Junctions

There are two types of junctions that are used in bond graphs, 0-junctions and 1-junctions. The 0-junctions have the property that all the bonds connected to the junction share a common effort and that the sum of the flows must equal zero. The signs are determined by the direction of the half arrows

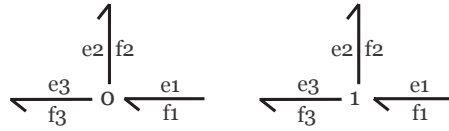


Figure 5.1: Junctions

in the bond graph. With respect to figure 5.1 this yields

$$e_1 = e_2 = e_3, f_1 - f_2 - f_3 = 0 \quad (5.1)$$

For 1-junctions the relationship is the opposite, the flow is common among the bonds and the sum of the efforts are zero, as expressed in Equation (5.2).

$$f_1 = f_2 = f_3, e_1 - e_2 - e_3 = 0 \quad (5.2)$$

Equations (5.1) and (5.2) both imply that the net power flowing into a junction is zero. Junctions are fundamental when it comes to translating a bond graph into a block diagram. The junctions shown in figure 5.1 are 3-port junctions. More than three ports can be created by combining two or more 3-ports.

5.1.5 2-port elements

Transformers and gyrators are 2-port elements, and are thus connected to two bonds. They are power conservative, just like the junctions are. For a transformer, the two efforts and the two flows are proportional to each other, as shown in Equation (5.3).

$$ae_1 = be_2, bf_1 = af_2 \quad (5.3)$$

The ratio b/a is called the modulus of the transformer. Gyrators are not as common as transformers, but the relationship between the power variables are included for the sake of completeness. Equation (5.4) shows how the efforts and the flows of a gyrator are related.

$$e_1 = rf_2, rf_1 = e_2 \quad (5.4)$$

5.2 Assignment of causality

An extensive explanation of causality is beyond the scope of this thesis. The focus will be on how to assign causality in a bond graph. Causality is determined by cause-effect relations. Each bond connects two elements in a bond graph, but it is not always easy to say whether element A (see



Figure 5.2: Assignment of causality

Table 5.3: Guidelines for causality assignment. Illustration: Rosenberg and Karnopp (1983)

Necessary causality	Se — Sf —
	— TF — or — TF —
	— GY — or — GY —
Restricted causality	$\begin{array}{c} \\ \text{--- o ---} \end{array}$ or $\begin{array}{c} \\ \text{--- o ---} \end{array}$ or $\begin{array}{c} \\ \text{--- o } \end{array}$
	$\begin{array}{c} \\ \text{--- 1 ---} \end{array}$ or $\begin{array}{c} \\ \text{--- 1 } \end{array}$ or $\begin{array}{c} \\ \text{--- 1 ---} \end{array}$
Integral causality	— I — C
Derivative causality	— I — C
Arbitrary causality	— R or — R

figure 5.2) prescribes an effort upon element B, which replies with a flow, or opposite. However, when it comes to assigning causality in a bond graph there are certain guidelines that can be followed, as shown in table 5.3. The causal stroke, |, is the bond graph symbol for causality.

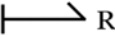

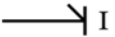
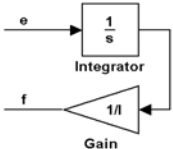
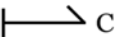
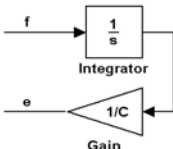
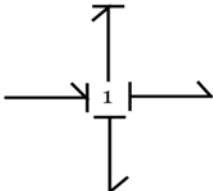
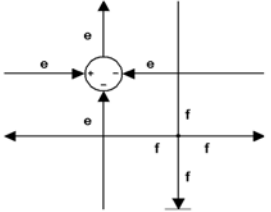
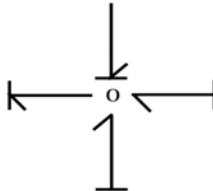
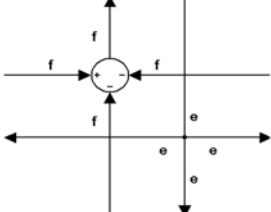

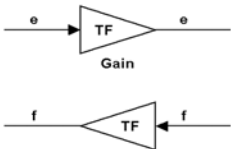

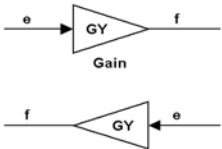

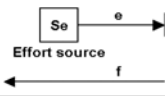

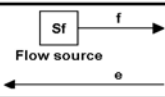
Sources are the easiest components to assign causality to, because there is only one option. An effort source creates an effort which is applied to another component, and therefore the causal mark must be placed at the far end of the bond connected to the source. The flow source produces a flow which causes the element at the other end of the bond to reply with an effort. Hence, the causality of the flow source is the opposite of the effort source. The causality of 2-ports and junctions are restricted, as shown in table 5.3. For 0-junctions only one bond can have the causal mark placed towards

the junction, while 1-junctions allow only one bond to have the causal mark placed away from the junction. Inertia and capacitor elements can have both integral and derivative causality, but integral causality is strongly preferred. The reason is that a realization of the elements will then involve integration instead of derivation. Resistor elements can be assigned whatever causality that fits. For a procedure on how to assign causality to bond graphs, see Samantaray (2005).

5.3 Converting bond graphs into block diagrams

A bond graph with causality and sign half arrows assigned to each bond contains all the necessary information to perform a simulation of the modeled system. To simulate in Simulink, however, the graph must first be converted to a suitable block diagram form. Table 5.4 shows the block diagram equivalents of the fundamental bond graph elements.

Table 5.4: Rules for converting bond graphs into block diagrams

Resistor		
Inertia		
Capacitor		
1-junction		
0-junction		
Transformer		
Gyrator		
Effort source		
Flow source		

Chapter 6

Modeling of the heave compensator system

The purpose of a heave compensation system is to isolate the motion of the load from the motion of the vessel (Perez and Steinmann, 2007). As explained in section 4 there exist both hydraulic and electric devices that are capable of this. The hydraulic configurations are the main concern of this chapter, but some parts describe concepts that apply to electric systems as well.

The Simulink model in this thesis is based on a bond graph of a hydraulic heave compensator (see figure 6.2). An advantage of this approach is that the system becomes modular, and it is therefore easy to remove and replace each part of the system with updated versions. Another reason for using a bond graph is that there are straightforward rules on how to convert the diagram into a Simulink model.

Figure 6.1 shows the main components of a hydraulic heave compensation system. This chapter focuses on developing mathematical models for the different parts. Subscript sh refers to the sheave with velocities measured relative to the mean free surface of the ocean, while subscript p refers to the pistons with velocities relative to the cylinder walls. The relative velocity between the pistons and the cylinder walls is calculated by $v_p = v_{sh} - v_{ve} = \dot{z}_{sh} - \dot{z}_{ve}$. Section 6.1 explains how the elongation of the cable can be modeled, while sections 6.2 and 6.3 give the equations of motion for the load and the sheave, respectively. It is assumed that the compliance of the system is concentrated in the passive and the active heave compensators. The dynamics of the winch, the pulleys and the overboard crane are therefore disregarded.

The objective of the servo control system is to keep the velocity of the load, V_{lo} , as close as possible to the winch velocity, V_{ca1} . Usually, the speed of the winch is constant. To achieve attenuation of the vessel motion, the pistons have to reciprocate out of phase with the heave motion. Due to the

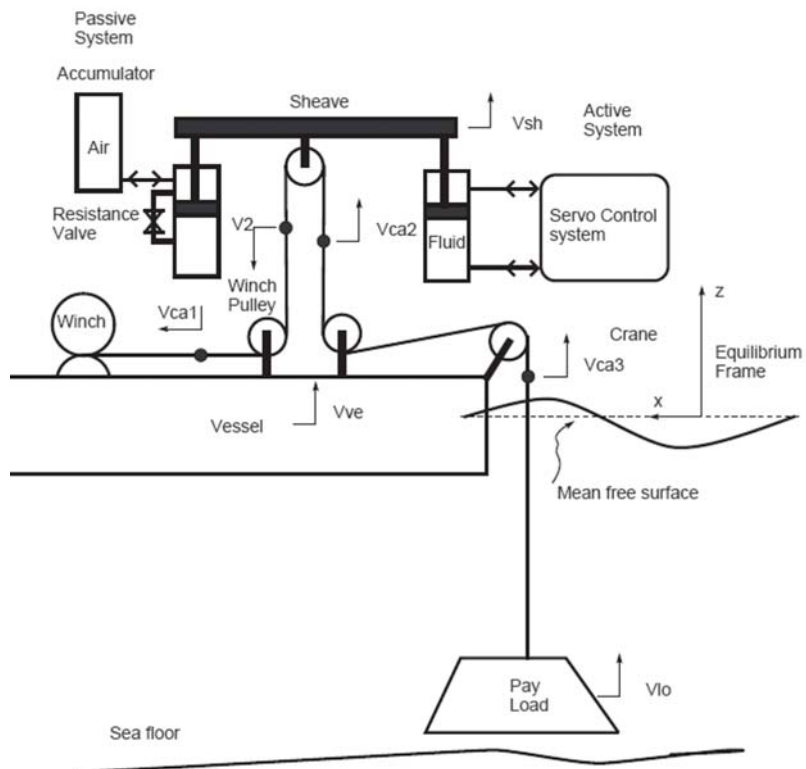


Figure 6.1: Schematic of a possible hydraulic heave compensator. Illustration: Perez and Steinmann (2007)

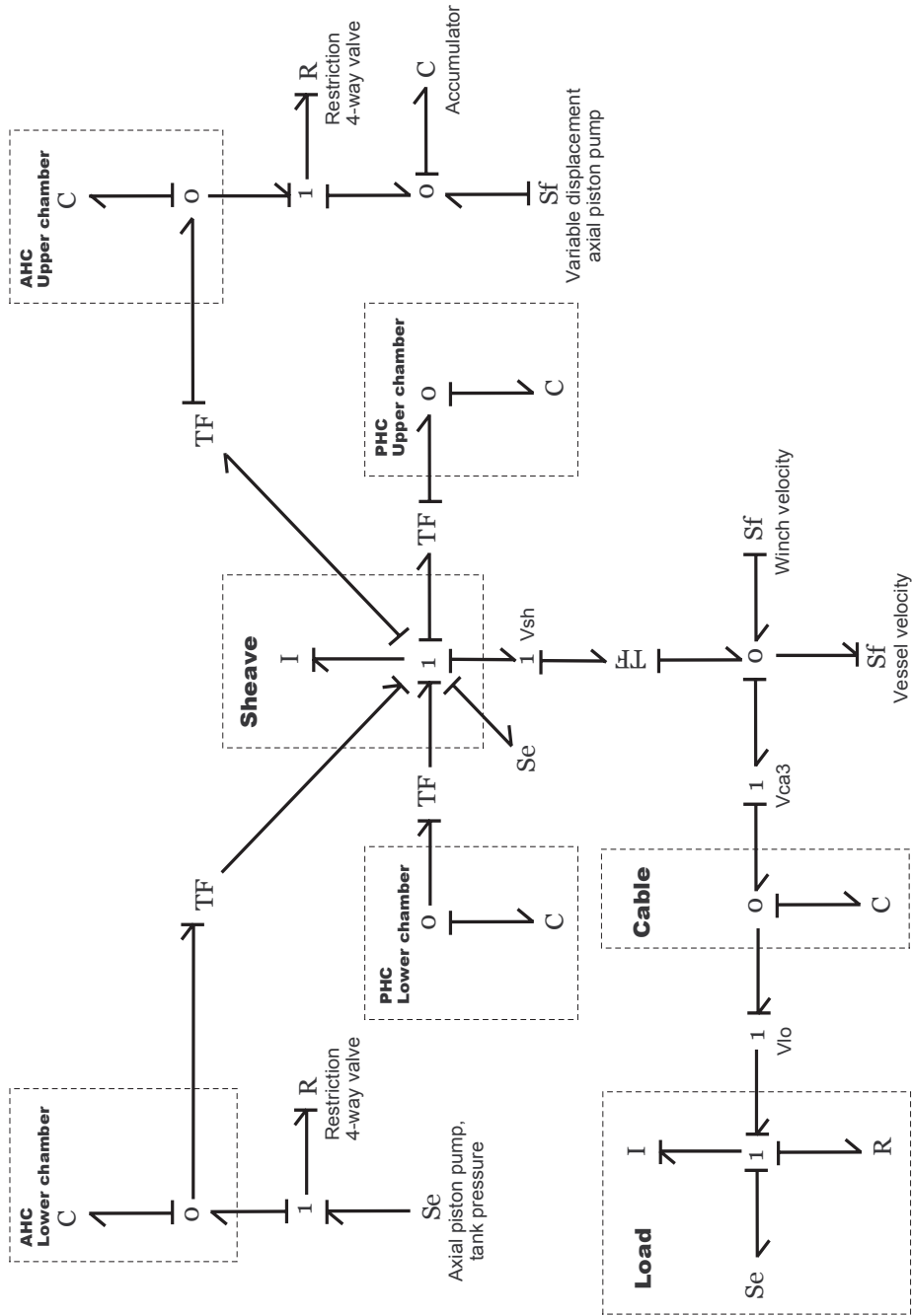


Figure 6.2: Bond graph of an hydraulic heave compensator. Illustration: Adapted from Perez and Steinmann (2007)

geometry of the system, perfect attenuation is obtained if

$$x_p(t) = -\frac{1}{2}z_{ve}(t) \quad (6.1)$$

where it is assumed that $x_p(0) = z_{ve}(0) = 0$. Here, $x_p(t)$ is the motion of the pistons relative to the cylinder walls and $z_{ve}(t)$ is the heave position of the vessel.

The motion of the load is also affected by the elongation of the cable. This means that even if the deviance between the desired and the actual piston motion is zero, the load may move up and down. How to reduce the oscillatory motion due to the cable elongation is elaborated on in section 6.7.

6.1 Modeling of the cable

To account for elasticity, the cable is modeled as a stiff spring. The force that the cable exerts is proportional to the ratio between the cable elongation, ΔL , and the unstretched length of the cable, L .

$$F_c = \frac{EA_0\Delta L}{L} = K_c\Delta L \quad (6.2)$$

Here, E is the modulus of elasticity and A_0 is the original cross-sectional area of the cable. The cross-sectional area is assumed to be unaffected by the elongation of the cable. Values for the modulus of elasticity is given in table 6.1 for two different materials. The spring stiffness

$$K_c = \frac{EA_0}{L}$$

varies with the cable length, and so does the natural frequency of the spring-damper-mass system consisting of the load and the cable. The latter is expressed in Equation (6.3).

$$\omega_c = \sqrt{\frac{K_c}{M_{lo} + M_c(L)}} \quad (6.3)$$

Traditionally, steel cables have been used, but as the desire to reach greater depths increase, the weight of the cable becomes increasingly important. At a depth of about 2000 meters the power consumption of the winch controlling the cable is doubled. The size and weight of a winch able to handle this amount of steel cable is also an issue, especially for smaller vessels. Therefore, use of High Modulus Polyethylene (HMPE) fibers is being investigated to be able to operate motion compensation and lifting systems for depths below 2000 meters. Honeywell has developed what they call Spectra fiber which is "10 times stronger than steel of equal weight, light-weight, naturally buoyant and resistant to wear-and-tear and degradation from water and most chemicals, as well as from ultraviolet radiation" (Costain and

Table 6.1: Modulus of elasticity

Steel	190-210 GPa
HMPE	172 GPa (Honeywell Spectra [®] fiber 1000)

Table 6.2: Load variables

Description	Variable name	Value
Load mass	M_{lo}	100tonnes
Cable mass	M_c	$\propto L$
Volume of displaced water	V_{disp}	$2m^3$
Density of water	ρ	$1003kg/m^3$
Load added mass	A_{lo}	0kg
Load drag coefficient	C_d	0.6
Load projected area	A_p	$1m^2$
Cable force	F_c	$\sim 9.6 \times 10^5$

Bull, 2006). Resistance to wear and tear, and especially bending, is important for hydraulic heave compensation systems as the rope has a continuous bend over the sheaves (see figure 4.2). In addition to the obvious advantages, the reduced weight of fiber rope systems will also result in significant cost savings due to increased vessel availability, as a wider range of vessels can be equipped with this kind of system. Faster deployment and recovery speeds are yet another important improvement. (Costain and Bull, 2006)

6.2 Equations of motion for the load

The motion of the load is modelled according to Newtons second law. Table 6.2 describes the relevant variables and the values used in this thesis. Some of the values are probably incorrect due to lack of data. Notice that the mass of the cable is proportional to the cable length. Viscous damping due to vortex shedding is the dominant damping force for the load. This is modeled as the second term in Morisson's equation (Fossen, 2002).

$$(M_{lo} + A_{lo})\ddot{z}_{lo} + D_{lo}(\dot{z}_{lo}) + (M_{lo} + M_c(L) - \rho V_{disp})g = F_c \quad (6.4)$$

$$D_{lo}(\dot{z}_{lo}) = \frac{1}{2}\rho C_d A_p |\dot{z}_{lo}| \dot{z}_{lo} \quad (6.5)$$

6.3 Equations of motion for the sheave

The motion of the sheave is affected by its weight, the cable force, the pressure forces inside the passive and the active cylinder, and internal forces such as viscous damping and friction inside the cylinders. Equation (6.6)

represents the equation of motion for the sheave, and p_{P1} and p_{P2} are the pressures in the lower and upper chambers of the passive cylinder, respectively. The same notation is used for the active cylinder.

$$\begin{aligned} M_{sh}\ddot{z}_{sh} &= F_{ext} + F_{int} \\ &= (-M_{sh}g - 2F_c + p_{P1}A_{P1} - p_{P2}A_{P2} \\ &\quad + p_{A1}A_{A1} - p_{A2}A_{A2}) - Bv_p \end{aligned} \quad (6.6)$$

The sheave is affected by twice the cable force due to the geometry of the cable laying (see figure 6.1). In Equation (6.6) the friction is not present. To account for the Coulomb friction, F_{ext} must be replaced by F_K according to the following expression

$$\begin{aligned} F_K &= 0 && \text{if } v_p = 0 \text{ and } |F_{ext}| < F_{cou} \\ F_K &= \text{sign}(F_{ext})(|F_{ext}| - F_{cou}) && \text{if } v_p = 0 \text{ and } |F_{ext}| \geq F_{cou} \\ F_K &= F_{ext} - \text{sign}(v_p)F_{cou} && \text{if } |v_p| > 0 \end{aligned}$$

where F_{cou} is the Coulomb friction coefficient. This expression is implemented in the Simulink model. The last term in Equation (6.6) accounts for the internal viscous friction in both the passive and the active cylinder, and the friction coefficient is given by

$$B = B_{phc} + B_{ahc} \quad (6.7)$$

where both B_{phc} and B_{ahc} are modeled according to Equation (6.8), but with different values for the bulk modulus, β . For the active cylinder, the bulk modulus for hydraulic fluid, $\beta_{ahc} = 7.0e8 Pa$ is chosen, while the passive cylinder has a value of $\beta_{phc} = 1.42e5$ which represents the compressibility of air. The lower the value, the more compressible the fluid is.

$$B_{hc} = 4A_p\zeta_h\sqrt{\frac{\beta m_t}{V_t}} \quad (6.8)$$

The relative damping has been set to $\zeta_h = 0.1$. According to Egeland and Gravdahl (2002) this parameter is typically in the range $0.1 \leq \zeta_h \leq 0.5$.

6.4 Passive heave compensation

The schematic in figure 6.1 is somewhat simplified. The passive cylinder is actually filled with hydraulic fluid and connected to an air fluid separator and an air accumulator. Because the compressibility of air is several times higher than for hydraulic fluid, it is assumed that the compression due to the motion of the piston is absorbed by the air alone. Therefore, the air fluid separator is not present in the figure, and the dynamics have been

neglected in the Simulink model. Due to fire hazard and oxidation, Kjølle (1995) suggests the use of nitrogen gas instead of air inside the separator.

Further, it is assumed that the system is isentropic, that is, there is no heat exchange with the environment. The work performed on the gas by the motion of the piston is stored as internal energy in the gas. For an ideal gas the internal energy is a function of temperature as shown in Equation (6.9) (Egeland and Gravdahl, 2002), where $c_v(T)$ is the specific heat at constant volume and T is the temperature in degrees Kelvin.

$$du = c_v(T)dT \quad (6.9)$$

If $c_v(T)$ is constant, the relationship is given by

$$\Delta U = c_v \Delta T \quad (6.10)$$

which shows that the temperature increases when the air is being compressed. Issues related to this temperature change are not considered in this thesis. The isentropic assumption together with the ideal gas law $pV = mRT$ leads to the isentropic relations (Egeland and Gravdahl, 2002)

$$\frac{T_2}{T_1} = \left(\frac{V_1}{V_2} \right)^{\kappa-1} \quad (6.11)$$

$$\frac{T_2}{T_1} = \left(\frac{p_2}{p_1} \right)^{\frac{\kappa-1}{\kappa}} \quad (6.12)$$

$$\frac{p_2}{p_1} = \left(\frac{V_1}{V_2} \right)^{\kappa} \quad (6.13)$$

where $\kappa := \frac{c_p}{c_v}$ is defined as the ratio between the specific heats at constant pressure and constant volume, respectively. Note that κ is also assumed to be constant. For diatomic gases $\kappa = 1.4$. The isentropic relations yields the pressure in the passive cylinder as shown in Equation (6.14).

$$p = \left[\frac{V_0}{V_0 + \int \dot{V} dt} \right]^{\kappa} p_0 \quad (6.14)$$

Here, the instantaneous volume of the pressurised air, $V = V_0 + \int \dot{V} dt$, has been substituted.

The slope of the graph in figure 6.3 corresponds to the compliance of the passive system. If the slope is very steep, a large pressure change is necessary to produce a small change in volume. The compliance will then be small. On the other hand, if the compliance is too high, the passive system could become oversensitive to the vessel motion and unsuitable as a backup in case the active system fails. It is therefore important to choose appropriate values for the volume and the initial pressure of the cylinder.

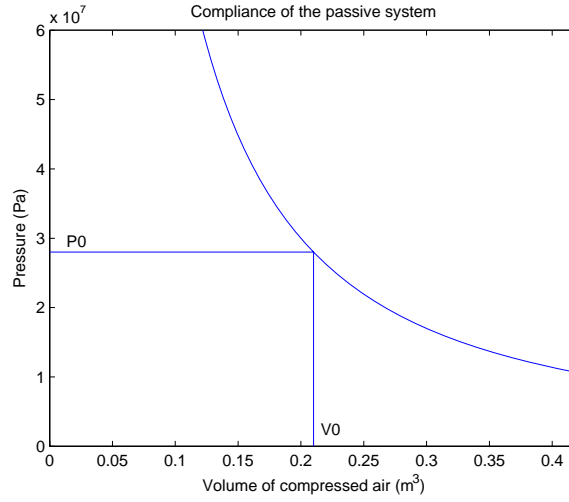


Figure 6.3: PV diagram for the compliance of the passive system

The main purpose of the passive cylinder is to relieve the active cylinder of the pressure created by the static load force. Therefore, the initial pressure inside the passive cylinder is set to balance the weight of the load in water plus the weight of the sheave and thus make the piston oscillate around its middle position. It is possible to manually or automatically tune the pressure inside the pneumatic accumulator while the system is operating. This is necessary because of leakage and change in the total weight when cable is payed out or taken in. With increasing pressure, the same load can be balanced using a cylinder with a smaller cross-sectional area, and thus the total size and weight of the passive system can be reduced. The pressure can only be increased until issues such as leakage, fluid temperature, acoustic noise and material strength become significant (Egeland, 1993). A smaller cross-sectional area reduce the volume of the cylinder and hence, the compliance is lowered (see figure 6.3).

The simulations in this thesis are based on the differential expressions in Equation (6.15) and (6.16) (Egeland and Gravdahl, 2002) instead of Equation (6.14). This gives the opportunity to develop the model further and avoid the assumption of isentropic conditions.

$$\frac{V_{10} + A_1 x_p}{\kappa} \dot{p}_1 = -A_1 \dot{x}_p p_1 \quad (6.15)$$

$$\frac{V_{20} - A_2 x_p}{\kappa} \dot{p}_2 = -A_2 \dot{x}_p p_2 \quad (6.16)$$

The performance of the passive heave compensator alone is acceptable but not very good. Figure 6.4 indicates that the reduction is about 50% for a 10

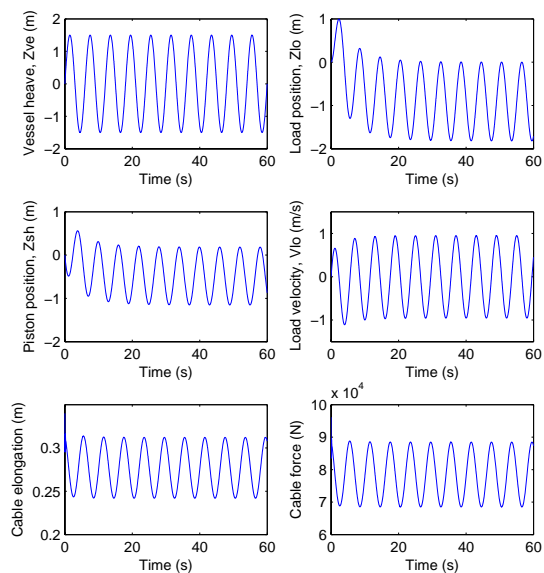


Figure 6.4: Passive system performance in sinusoidal waves with a 10 tonnes load and a 500 meter cable.

tonnes load. The heavier the load, the more energy from the vessel motion is absorbed by the passive system and less is transferred to the load. This is illustrated in figure 6.5. It may be possible to achieve better results by optimizing the dimensions of the cylinder and the air accumulator.

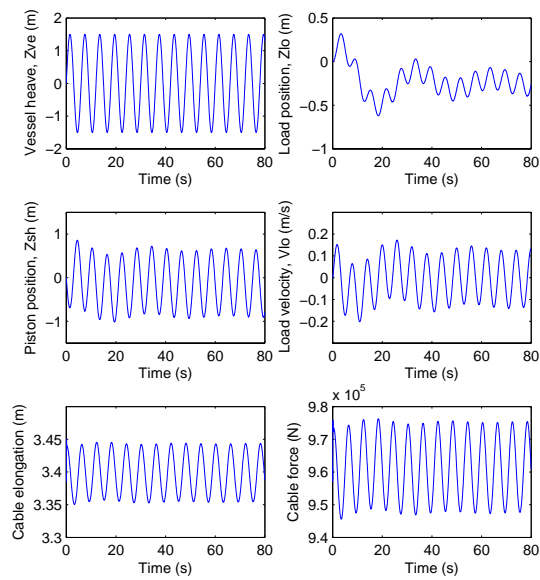


Figure 6.5: Passive system performance in sinusoidal waves with a 100 tonnes load and a 500 meter cable.

6.5 Active heave compensation

The servo control system shown in figure 6.1 consists of the following components:

Tank filled with hydraulic fluid at atmospheric pressure

Filter to keep impurities from entering the system

Axial piston pump with variable displacement

Control loop adjusting the angle of the pump swashplate to keep the supply pressure for the servo valve constant

Servo valve to control the fluid flow in and out of the active cylinder

In addition to the servo control system, the active heave compensator includes a hydraulic cylinder. The cylinder needs to be properly dimensioned, and this is explained in the next section.

6.5.1 Static dimensioning

The motion compensation system must be designed to meet certain requirements given by the mass of the load and the amplitude and frequency of the waves. In this section it is assumed that the passive compensator is not present, such that the active system has to carry the whole weight of the load. With the geometry shown in figure 6.1, it must be able to support the weight of the sheave plus twice the weight of the load. A reasonable margin of safety should also be included. The maximum force, F_{max} , the pressure drop, p_L , across the cylinder piston, and the coefficient of efficiency, η_{mh} , determine the effective piston area according to Equation (6.17) (Kjølle, 1995). The efficiency coefficient includes the losses due to internal friction in the cylinder. It is important to calculate the dimensions of the cylinder based on the weight of the heaviest load it is designed to support. If the heave compensator is overloaded, the consequence could be that the flow into the cylinder saturates and the system becomes unstable.

$$A_p = \frac{F_{max}}{p_L \eta_{mh}} \quad (6.17)$$

In valve controlled systems it is desirable to dimension the valve such that the flow rate is large enough to retain precise control. According to Egeland and Gravdahl (2002), the load flow of a matched and symmetric valve with a symmetric load can be expressed by

$$q_L = C_d b x_v \sqrt{\frac{1}{\rho} (p_s - \text{sgn}(x_v) p_L)} \quad (6.18)$$

where C_d is the discharge coefficient, x_v is the spool position of the valve, b is the flow area coefficient, p_s is the supply pressure and $p_L = p_1 - p_2$ is the load pressure. For a hydraulic cylinder the load pressure is the pressure drop across the piston. It is assumed that the pressure in the return tank is equal to the ambient atmospheric pressure, and thus the gage pressure is $p_r = 0$.

The assumption of a symmetric load implies that the flow into and out of the cylinder is equal, and thus, compressibility of the hydraulic fluid is not accounted for (Egeland and Gravdahl, 2002). The reason for making this assumption is that it yields simple transfer functions with sufficiently small errors to be used in static dimensioning and model verification.

It is common practice to decide upon a suitable supply pressure and dimension the system such that the load pressure will be limited by $|p_L| < \frac{2}{3}p_s$. This is motivated by calculating the maximum power delivered through the valve. The power is given by

$$P = q_L p_L = C_d b x_v \sqrt{\frac{1}{\rho} (p_s - \text{sgn}(x_v) p_L) p_L} \quad (6.19)$$

and the load pressure which yields the maximum power is found by

$$\frac{dP}{dp_L} = C_d b x_v \sqrt{\frac{1}{\rho}} \left[\sqrt{p_s - \text{sgn}(x_v) p_L} - \frac{p_L}{2} \frac{1}{\sqrt{p_s - \text{sgn}(x_v) p_L}} \right] = 0 \quad (6.20)$$

Equation (6.20) gives $|p_L| < \frac{2}{3}p_s$. This load pressure can then be used in Equation (6.17) to determine the area of the cylinder piston. Another reason to limit the load pressure is that the pressure-flow curves are close to linear in this range (Egeland and Gravdahl, 2002).

To obtain satisfactory motion compensation, the maximum velocity of the cylinder piston must be sufficiently large. The necessary speed is given by the slope of the waves and the valve must be able to deliver a flow rate of

$$Q_{max} = A_p v_{p_{max}} \quad (6.21)$$

where $v_{p_{max}}$ is the maximum velocity of the piston necessary to attenuate the motion of the vessel. In the four way valve shown in figure 6.6, the fluid passes through the valve twice for a given spool position. The remainder of the supply pressure not distributed across the cylinder piston is divided equally over the two passes. This is a consequence of the assumptions specified above (Kjølle, 1995). The pressure drop for each pass then becomes $\Delta p = \frac{p_s - p_L}{2} = \frac{1}{6}p_s = \frac{1}{4}p_L$ and the flow rate through the valve is given by

$$Q = C_d A_v \sqrt{\frac{2\Delta p}{\rho}} = C_d A_v \sqrt{\frac{p_L}{2\rho}} \quad (6.22)$$

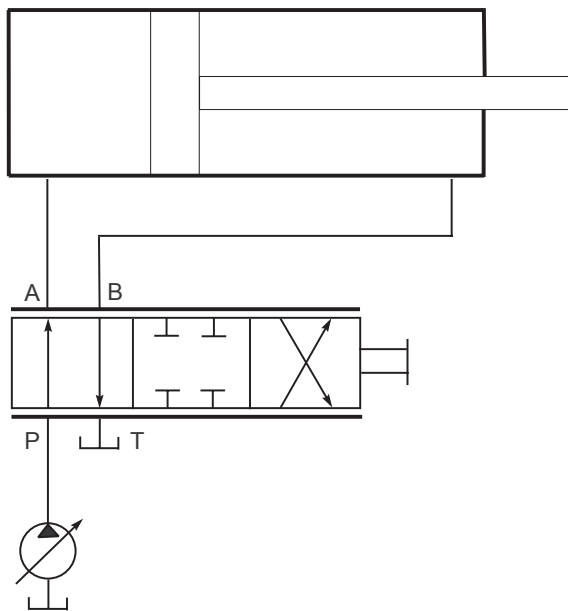


Figure 6.6: Schematic of double-acting cylinder controlled by a four-way valve

The flow area required to deliver a flow rate of $Q = Q_{max}$ is thus (Kjølle, 1995)

$$A_{v_{max}} = \frac{Q_{max}}{C_d \sqrt{\frac{p_L}{2\rho}}} \quad (6.23)$$

and the flow area coefficient b is found by

$$b = \frac{A_{v_{max}}}{x_{v_{max}}} \quad (6.24)$$

where $x_{v_{max}}$ is the maximum displacement of the piston inside the valve.

6.5.2 Transfer function and control law

According to Egeland and Gravdahl (2002) the mass balances for the two chambers of the cylinder and the equation of motion for the piston yields the following dynamic model for the active system

$$\frac{V_{10} + A_1 x_p}{\beta} \dot{p}_1 = -C_{im}(p_1 - p_2) - C_{em} p_1 - A_1 \dot{x}_p + q_1 \quad (6.25)$$

$$\frac{V_{20} - A_2 x_p}{\beta} \dot{p}_2 = -C_{im}(p_2 - p_1) - C_{em} p_2 + A_2 \dot{x}_p - q_2 \quad (6.26)$$

$$m_t \ddot{x}_p = -B_p \dot{x}_p + A_1 p_1 - A_2 p_2 - F_L \quad (6.27)$$

Here q_1 and q_2 are the flows in and out of the two chambers, C_{im} and C_{em} represent the internal leakage and the motor leakage respectively, m_t is the mass of the piston and the sheave, B_p is the viscous friction coefficient, and $F_L = 2F_c$ is the load force.

If the cylinder is matched and symmetric and the load is assumed to be symmetric, Equations (6.25) and (6.26) can be combined to yield (Egeland and Gravdahl, 2002)

$$\frac{V_t}{4\beta} \dot{p}_L = -C_{tp} p_L - A_p \dot{x}_p + q_L \quad (6.28)$$

where

$$\begin{aligned} V_t &= V_{10} + V_{20} \\ p_L &= p_1 - p_2 \\ C_{tp} &= C_{im} + \frac{1}{2} C_{em} \\ q_L &= \frac{1}{2} (q_1 + q_2) \end{aligned}$$

A symmetric cylinder means that the upper and lower piston areas are the same. In the simulations in this thesis the areas are actually different, so the theoretical value A_p is taken as the average of A_1 and A_2 , that is $A_p = \frac{A_1 + A_2}{2}$.

Linearization of the valve characteristic in Equation (6.18) gives

$$q_L = K_q x_v - K_c p_L \quad (6.29)$$

where $K_q = \frac{\partial q_L}{\partial x_v}$ and $K_c = -\frac{\partial q_L}{\partial p_L}$ are the coefficients of linearization. The complete linear model can then be expressed by

$$\frac{V_t}{4\beta} \dot{p}_L = -C_{tp} p_L - A_p \dot{x}_p + q_L \quad (6.30)$$

$$m_t \ddot{x}_p = -B_p \dot{x}_p + A_1 p_1 - A_2 p_2 - F_L \quad (6.31)$$

$$q_L = K_q x_v - K_c p_L \quad (6.32)$$

By assuming no leakage and $B_p \neq 0$, the Laplace transform of the model becomes (Egeland and Gravdahl, 2002)

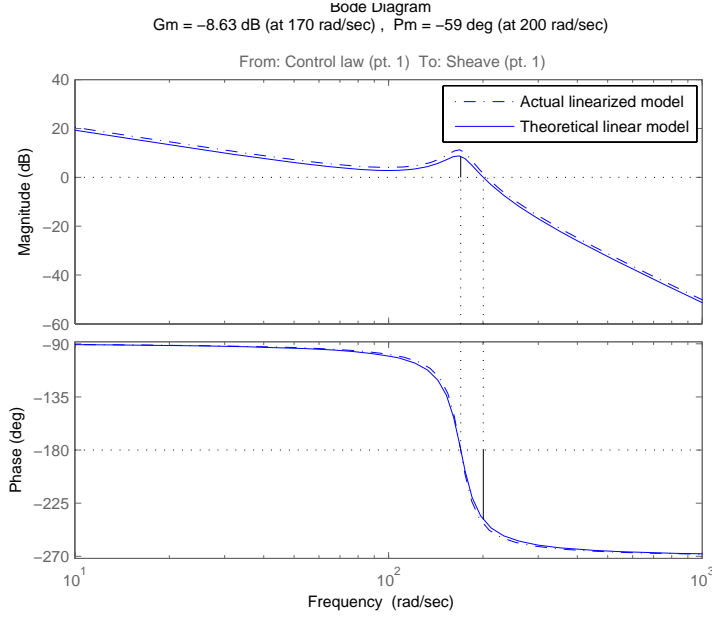


Figure 6.7: Comparison between theoretical and actual model

$$x_p(s) = \frac{\frac{K_q}{A_p} x_v(s) - \frac{K_{ce}}{A_p^2} \left(1 + \frac{s}{\omega_t}\right) F_L(s)}{s \left(1 + 2\zeta_h \frac{s}{\omega_h} + \frac{s^2}{\omega_h^2}\right)} \quad (6.33)$$

where

$$K_{ce} = K_c + C_{tp} \quad (6.34)$$

$$\omega_h^2 = \frac{4\beta A_p^2}{V_t m_t}, \quad \zeta_h = \frac{B_p}{4A_p} \sqrt{\frac{V_t}{\beta m_t}}, \quad \omega_t = \frac{4\beta K_{ce}}{V_t} \quad (6.35)$$

The theoretical value for the natural frequency, ω_h , becomes 170 rad/s , which is exactly the same as the value calculated from a linear analysis of the Simulink model. Typical values for the relative damping, ζ_h , are between 0.1 and 0.5. In the simulations, the value for ζ_h has been set to 0.1 and the viscous friction coefficient, B_p , has been calculated using Equation (6.8). A bode diagram comparison between the theoretical and the actual model is shown in figure 6.7. The similarity can be seen as an indication of the correctness of the Simulink model.

Nyquist stability theory states that a system is stable as long as the gain of the loop transfer function at the frequency ω_{180} is less than or equal to 0dB. This is the frequency at which the frequency response of the loop

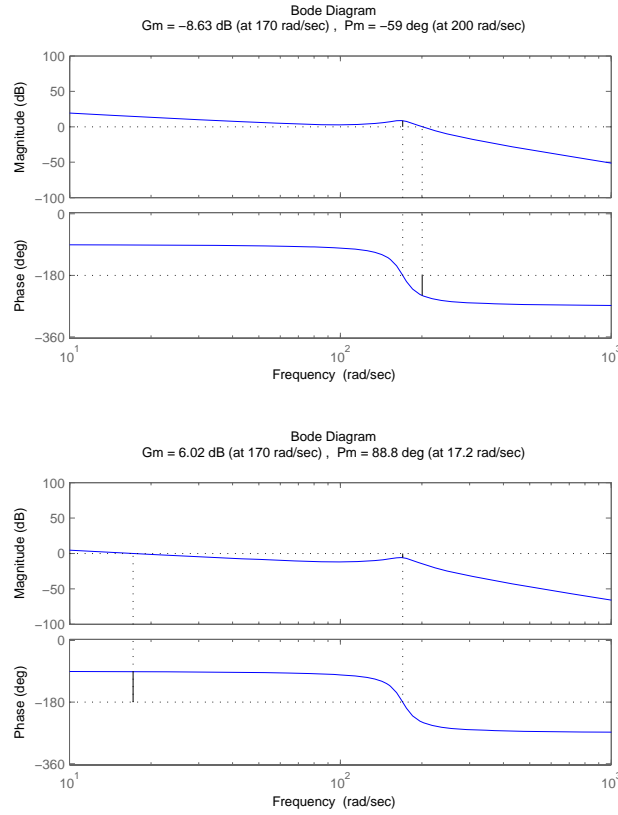


Figure 6.8: Bode diagram of the theoretical AHC loop transfer function. Upper: Only the AHC subsystem. Lower: With proportional controller

transfer function has a phase of 180° . With a proportional controller of the form $x_v = K_p(x_d - x_p)$, it can be seen that stability is ensured if (Egeland and Gravdahl, 2002)

$$K_p \leq 2 \frac{A_p}{K_q} \zeta_h \omega_h \quad (6.36)$$

and a 6dB gain margin is obtained with

$$K_p = \frac{A_p}{K_q} \zeta_h \omega_h \quad (6.37)$$

Figure 6.8 presents this result in a bode diagram. The simulations, however, show that the proportional gain, K_p , can be increased far beyond the theoretical value from Equation (6.37). This is probably due to additional damping introduced by the passive heave compensator.

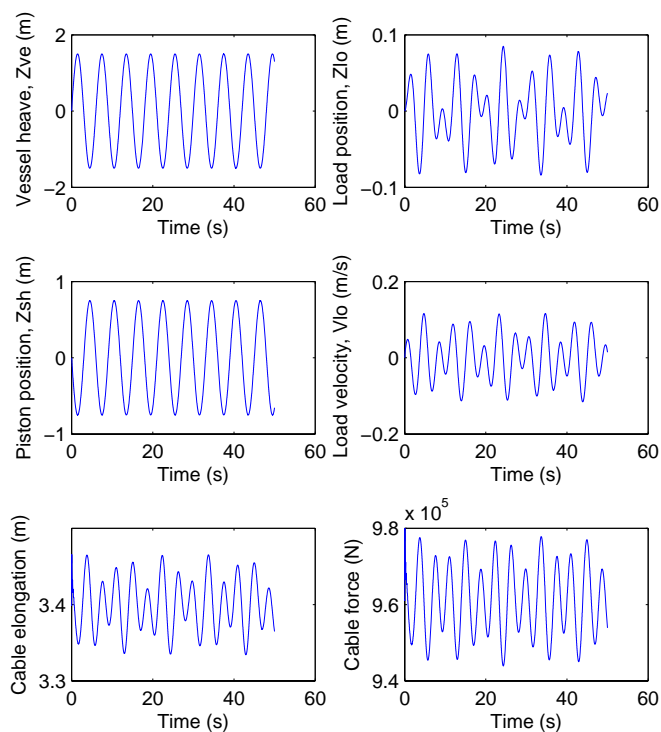


Figure 6.9: System behavior with 500 meter cable

6.6 Performance in regular waves

The system behavior for regular seas with a 100 tonnes load is shown in figures 6.9-6.12. The attenuation is between 86% and 97%. It can be seen that most of the load motion is due to the cable elongation. By tuning the value of K_p and introducing cable tension feedback, it is likely that even better results can be obtained.

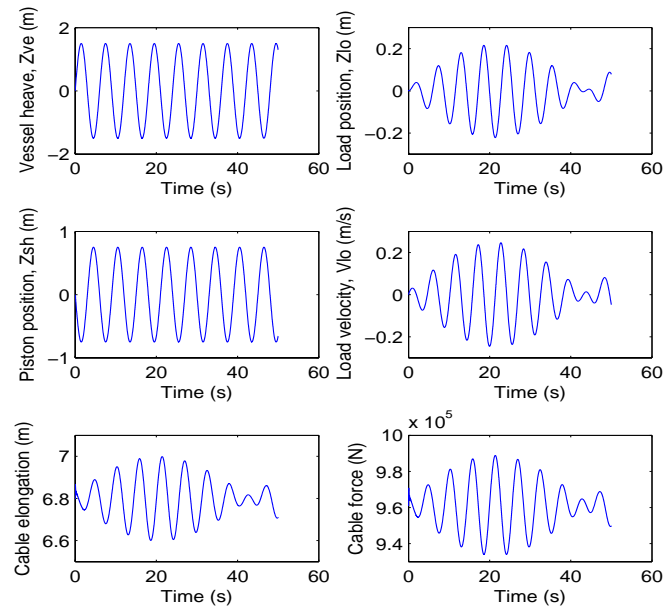


Figure 6.10: System behavior with 1000 meter cable

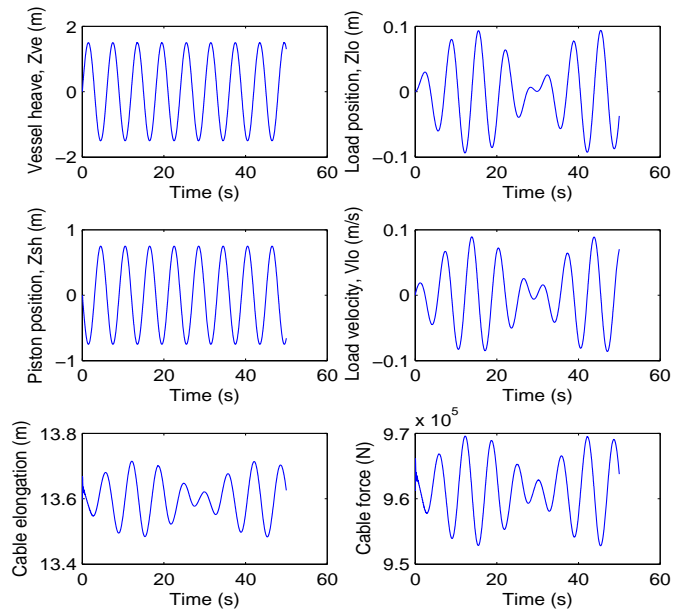


Figure 6.11: System behavior with 2000 meter cable

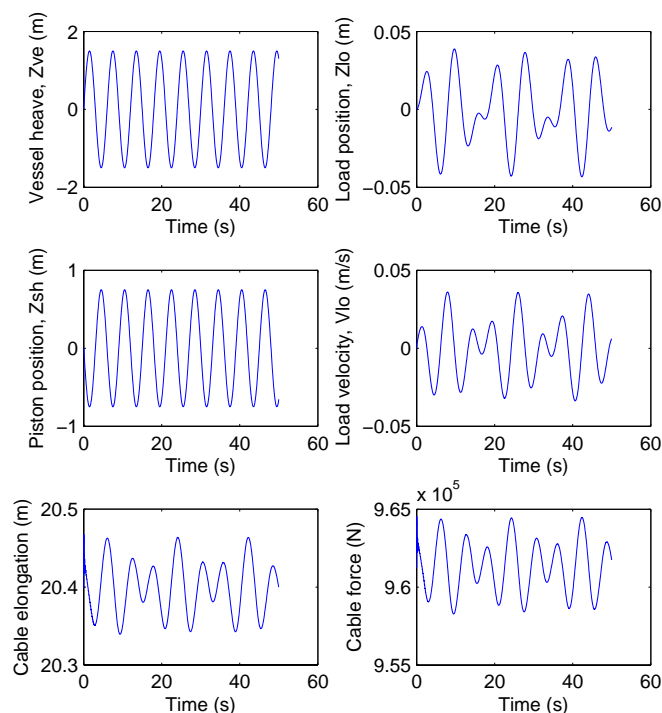


Figure 6.12: System behavior with 3000 meter cable

6.7 Performance in irregular waves

Figure 6.13 shows that there are two dominant frequencies in the motion spectrum of the load. The one to the left corresponds to the modal frequency of the irregular waves as defined in Equation (2.8), and the other is the natural frequency of the cable and load. The latter carries a lot of energy and it is clearly visible in figures 6.14 and 6.15. When the velocity of the load is small there is hardly any damping of this natural frequency in the system. For short cable lengths (stiff cable) or light mass the frequency will then propagate through the heave compensator and excite the cable-load system causing resonant behavior and instability, as shown in figure 6.15. A solution is to introduce artificial damping in the controller to try to keep the cable force and elongation constant. By adding feedback from the time integration of the deviation from constant cable tension, the energy of the natural frequency is greatly reduced (see figure 6.16). The system behavior with cable tension feedback is shown in figures 6.17 and 6.18. The attenuation is above 98%. Using feedback from the integrated tension is an

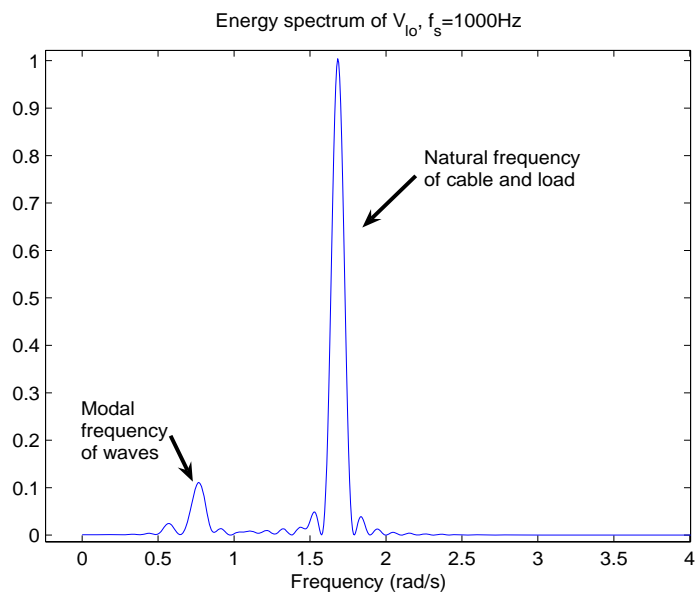


Figure 6.13: Load velocity frequency content without cable tension feedback

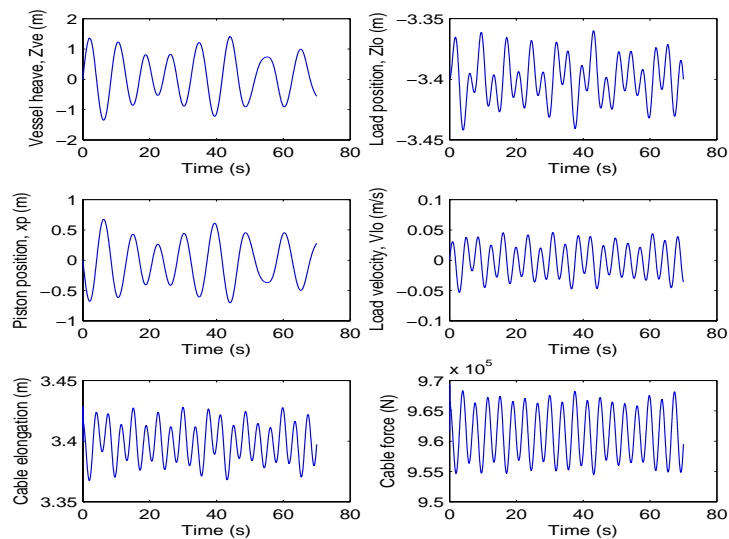


Figure 6.14: System behavior for irregular seas with 500 meter cable

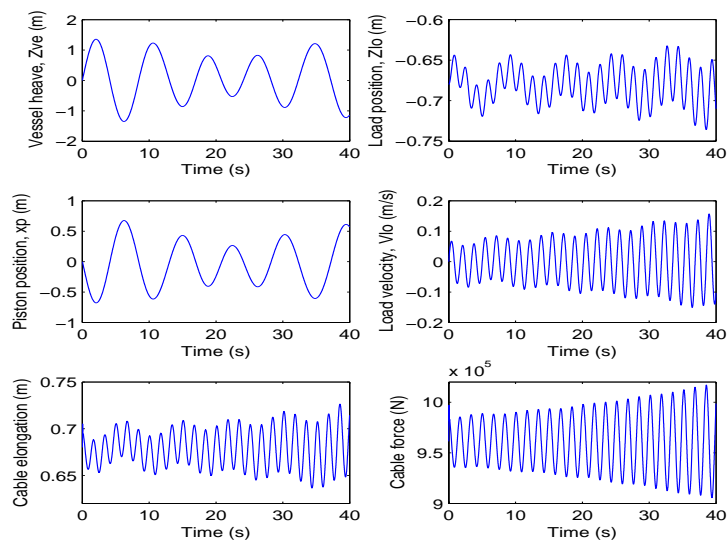


Figure 6.15: System behavior for irregular seas with 100 meter cable

idea taken from Skaare (2004).

Pure integrator feedback from the cable tension deviation is not sufficient for cable lengths of 10 meters or less. Simulations indicate that additional proportional feedback is necessary. The results for a 100 tonnes load attached at the end of a 10 meter cable is shown in figure 6.19.

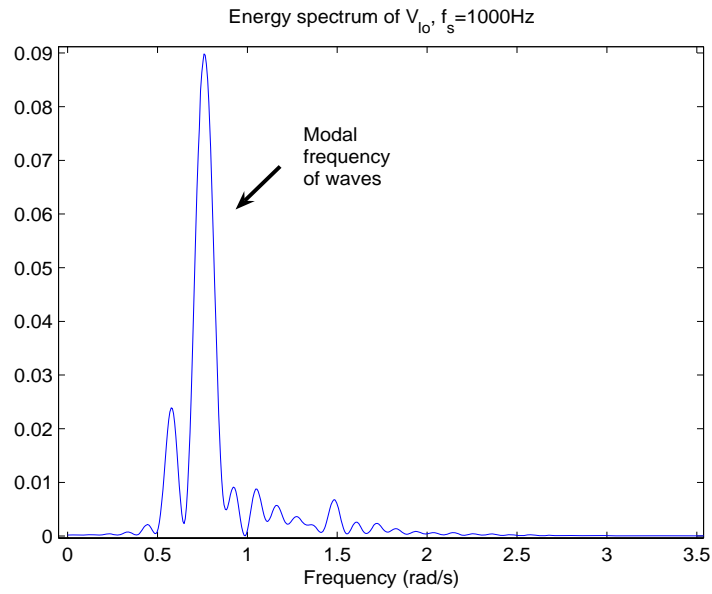


Figure 6.16: Load velocity frequency content with cable tension feedback

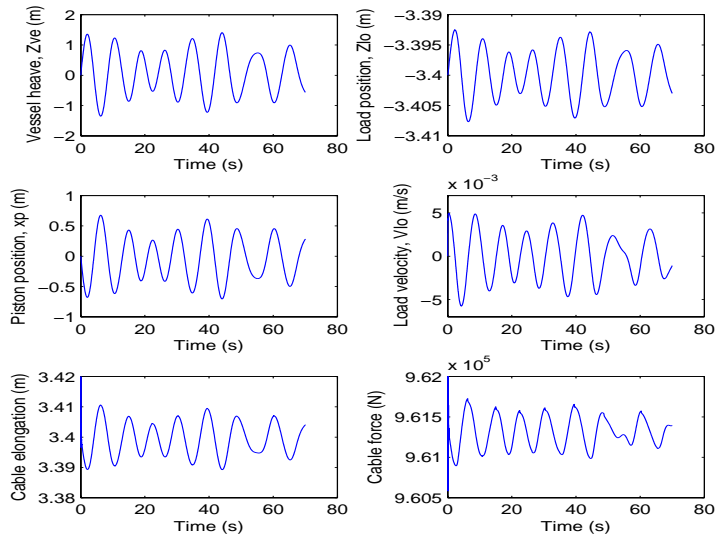


Figure 6.17: System behavior with cable tension feedback and 500 meter cable

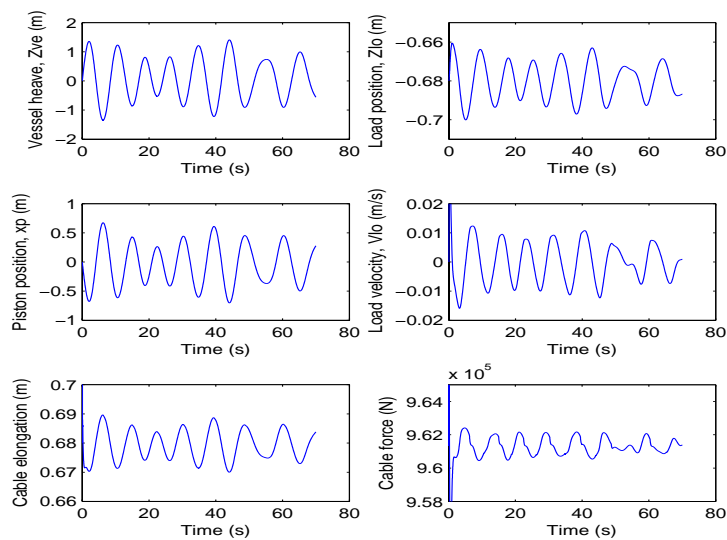


Figure 6.18: System behavior with cable tension feedback and 100 meter cable

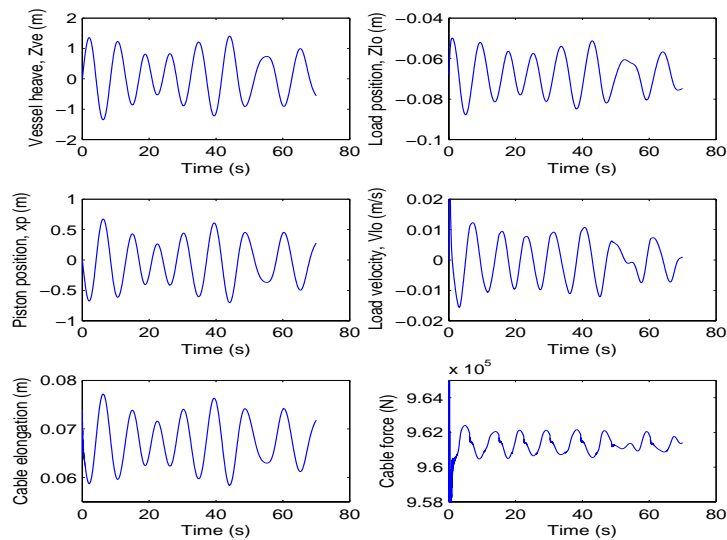


Figure 6.19: System behavior with cable tension feedback and 10 meter cable

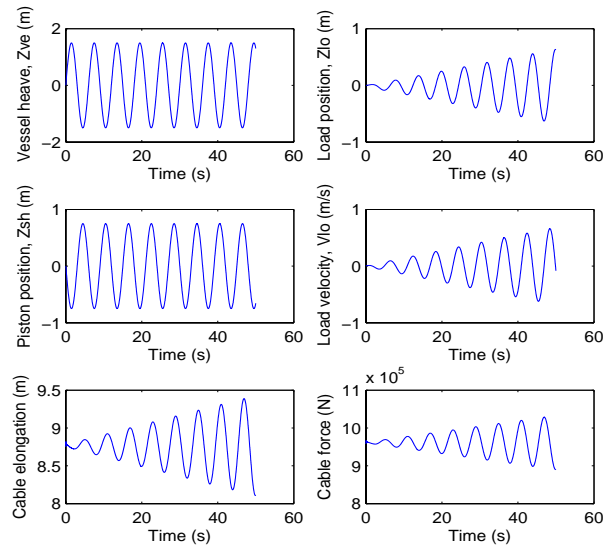


Figure 6.20: Resonant behavior in regular seas. Load mass 100 tonnes. Cable length 1289 meters.

6.8 Undesirable scenarios

This section explains and illustrates two scenarios that are important to handle in a safe manner or to avoid altogether.

6.8.1 Resonance

The two dominant frequencies shown in figure 6.13 will cause resonance if they get too close. As the cable length and the load mass increase, the natural frequency, ω_c , is reduced. In regular seas with a 100 tonnes load and a wave peak period of 6 seconds, the theoretical resonance occurs at a cable length of approximately 1289 meter. This calculation is made without regard to the mass of the cable. The result is shown in figure 6.20, and it can be seen that the system becomes unstable. For irregular seas with an average wave period of 6 seconds, the modal frequency of the waves coincides with the natural frequency of the cable-load system for a cable length of 2166 meters, as shown in figure 6.21. Figures 6.20 and 6.22 show that the motion of the piston still compensates for the vessel heave, but the cable elongation affects both the cable force and the load position. A worst case scenario is that the cable force becomes too large and the cable breaks. Snap loads in the cable will occur if the elongation becomes negative.

Resonance-like behavior is present also at cable lengths of 1000 meters

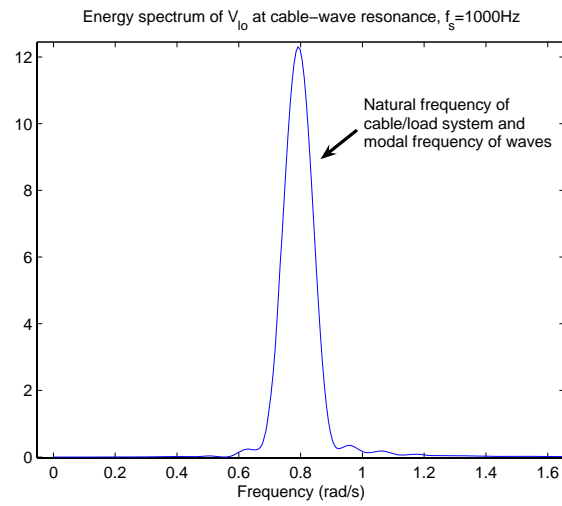


Figure 6.21: Load velocity frequency content at cable-wave resonance

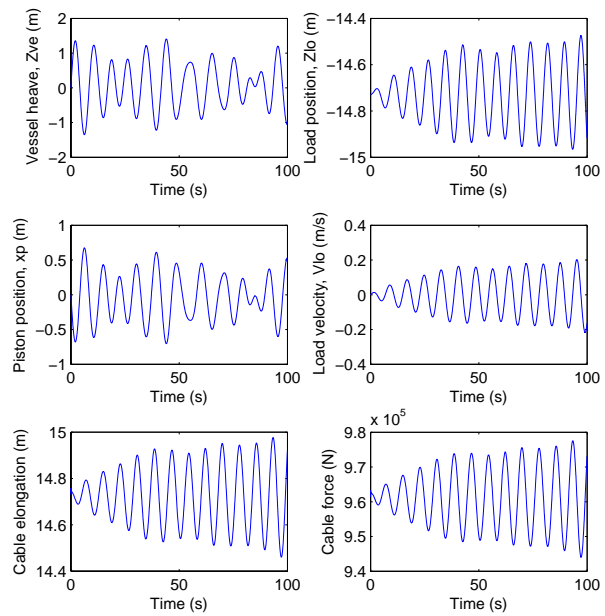


Figure 6.22: Resonant behavior in irregular seas. Load mass 100 tonnes. Cable length 2166 meters.

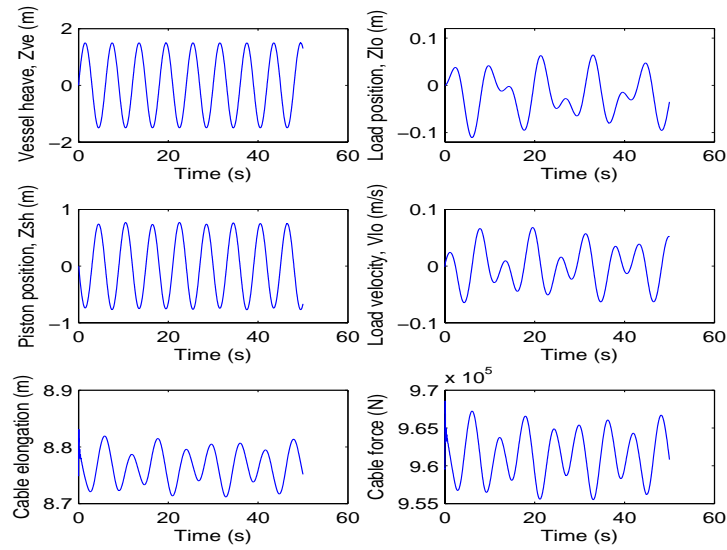


Figure 6.23: Behavior in regular seas with a 1289 meter cable and cable tension feedback

and 2000 meters (see figures 6.10 and 6.11). One way to avoid the resonance altogether is to turn off the heave compensator while the length of the cable is within the resonance range. Simulations indicate that there is another feasible solution. By introducing cable tension feedback, as explained in section 6.7, the energy corresponding to the natural frequency is diminished. Figures 6.23 and 6.24 show that this alleviates the resonance problems. The oscillations in the cable elongation and the cable force are reduced, and the load position is stabilized.

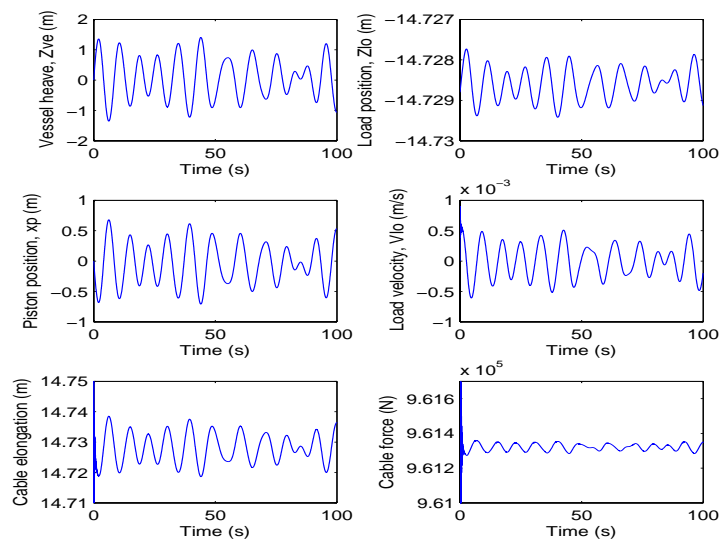


Figure 6.24: Behavior in irregular seas with a 2166 meter cable and cable tension feedback

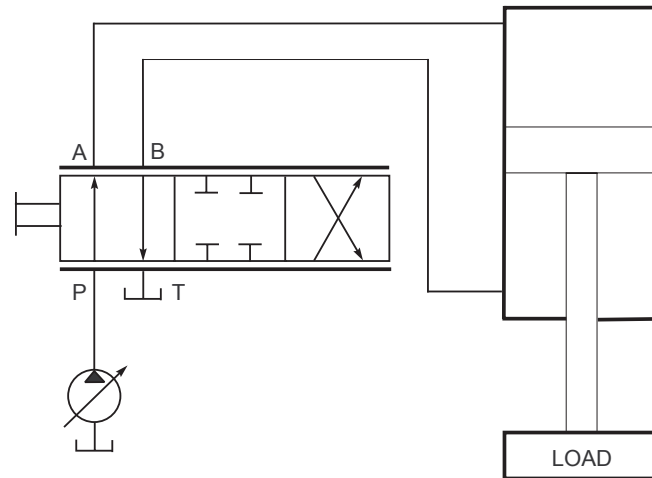


Figure 6.25: Schematic of a hanging load system without balance valve. Reproduced from Brautaset (1983).

6.8.2 Loss of supply pressure

A schematic of a hanging load system without balance valve is shown in figure 6.25. If the supply pressure is suddenly lost or greatly reduced, control of the piston motion is lost (shown to the left in figure 6.26). A solution is to switch the four way valve to its middle position to hydraulically lock the piston, but this results in a large pressure rise. (Brautaset, 1983)

Installing a balance valve, also called a back-pressure valve, is a better way to solve the problem. The balance valve is in general a pressure relief valve with a built-in check valve (see figure 6.27). The pressure relief valve generates a back-pressure to compensate the weight of the load and prevent it from running wild (Brautaset, 1983). An adjustable spring is used to set the desired back-pressure. According to Kjølle (1995) the back-pressure should be 1,3 times the load pressure. Brautaset (1983), however, suggests using a factor of 5. An arrangement like this enables the downward motion of the piston to be controlled by directing pressure energy into the upper chamber of the cylinder (Kjølle, 1995). In case the supply pressure is lost, the balance valve will close and the piston will be locked. This is shown to the right in figure 6.26. The purpose of the check valve is to direct the flow past the pressure relief valve when the direction of flow is reversed.

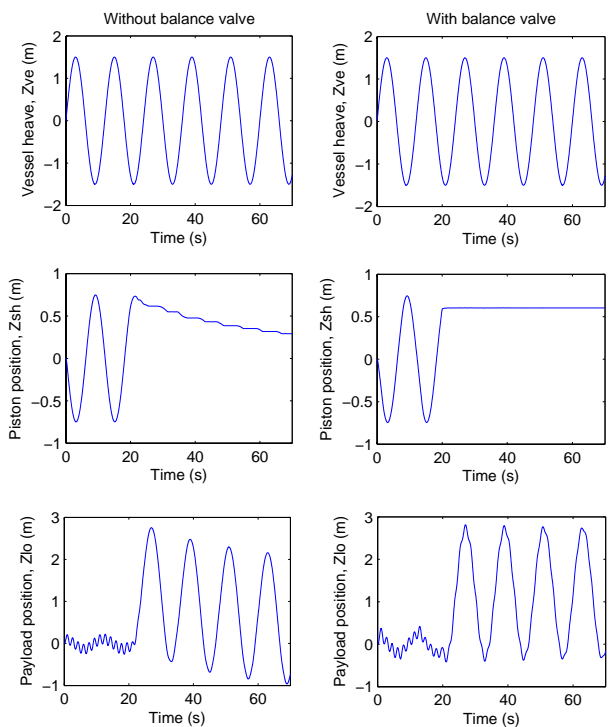


Figure 6.26: Response upon loss of supply pressure

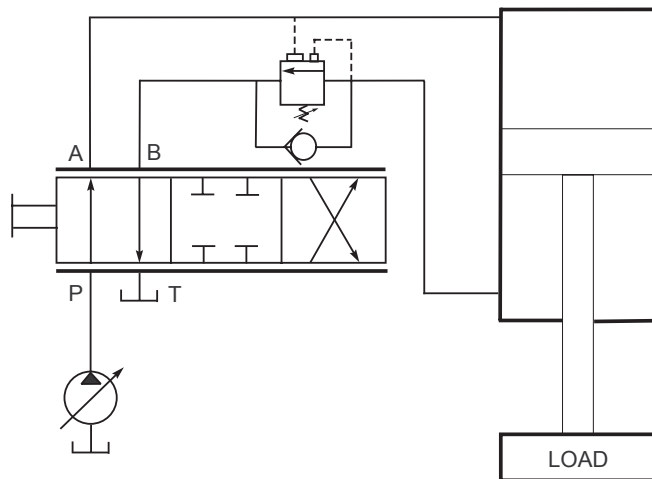


Figure 6.27: Schematic of a hanging load system with balance valve. Reproduced from Brautaset (1983).

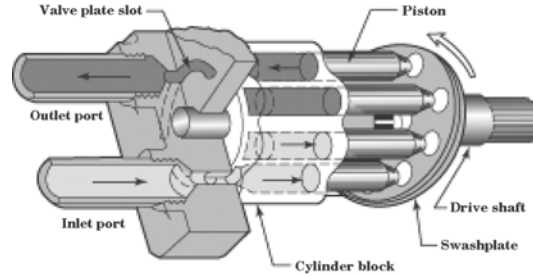


Figure 6.28: In-line piston pump. Illustration: Penton Media (n.d.).

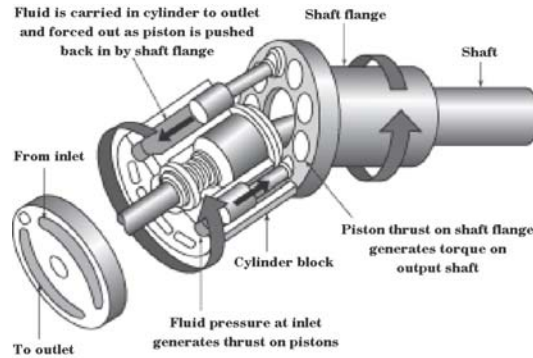


Figure 6.29: Principle for a bent axis piston pump (shown as a hydraulic motor). Illustration: Penton Media (n.d.).

6.9 Control loop for a pump with variable displacement

The four way valve and the hydraulic cylinder are dimensioned with respect to a given supply pressure. It is therefore desirable to keep the supply pressure close to constant. This can be achieved by using a pump with variable displacement. If an axial piston pump is considered, there are in general two ways to change the displacement, either by changing the angle of the swashplate inside the pump or by varying the angle between the motor shaft and the cylinder block. Figures 6.28 and 6.29 illustrate the two principles. The first type, also called an inline piston pump, tolerate a higher motor speed, but the latter has the advantage of a larger range of motion (Brautaset, 1983).

The inline piston pump is selected for the simulations in this thesis. An extra control loop is then added to vary the angle of the swashplate inside the pump. For simplicity, a proportional controller is chosen and the dynamics of the swashplate and the motor driving the pump are neglected. A change

of angle is thus assumed to happen instantaneously. The load torque applied to the motor actually depends on the pressure difference between the inflow and outflow chambers of the pump, but it is assumed that the motor includes its own controller to keep the shaft speed constant.

A simple explanation of how an axial piston pump works is given in Penton Media (n.d.):

"The pistons in an axial piston pump reciprocate parallel to the centerline of the drive shaft of the piston block. That is, rotary shaft motion is converted into axial reciprocating motion. Most axial piston pumps are multi-piston and use check valves or port plates to direct liquid flow from inlet to discharge.

The simplest type of axial piston pump is the swashplate design in which a cylinder block is turned by the drive shaft. Pistons fitted to bores in the cylinder block are connected through piston shoes and a retracting ring, so that the shoes bear against an angled swashplate.

As the block turns, the piston shoes follow the swashplate, causing the pistons to reciprocate. The ports are arranged in the valve plate so that the pistons pass the inlet as they are pulled out and the outlet as they are forced back in. In these pumps, displacement is determined by the size and number of pistons as well as their stroke length, which varies with the swashplate angle.

In variable displacement models of the inline pump, the swashplate swings in a movable yoke. Pivoting the yoke on a pintle changes the swashplate angle to increase or decrease the piston stroke. The yoke can be positioned with a variety of controls, i.e., manual, servo, compensator, handwheel, etc."

Figure 6.30 shows how a proportional controller keeps the supply pressure close to the desired value of 350 bar. The deviation is due to variations in the required flow rate, and the pattern repeats itself with the same frequency as the wave frequency.

If a pump with fixed displacement is chosen, it is a waste of energy to dimension it such that the maximum flow rate is equal to the peaks of the required flow rate. A better option is then to dimension the pump to supply the average required flow rate and add an accumulator to take care of the fluctuations. (Kjølle, 1995)

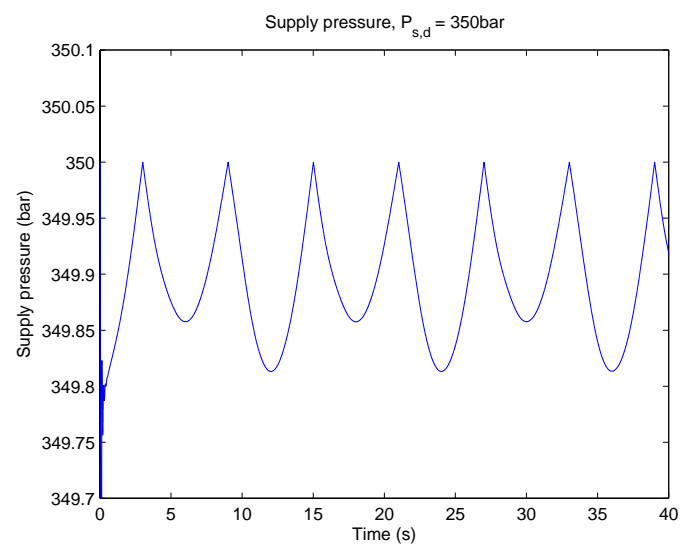


Figure 6.30: Supply pressure, desired value 350bar

Chapter 7

Conclusion and further work

7.1 Conclusion

This thesis has focused on heave compensation of offshore cranes. Both electric and hydraulic configurations have been considered, but the emphasis has been on hydraulic heave compensation. A Simulink model of a heave compensator was developed using the bond graph formalism. Both an active and a passive system were implemented, the passive system being modeled as a pneumatic damper and the active system as a closed-loop system consisting of a hydraulic cylinder and a servo valve control system. A wave spectrum for long-crested waves was created from the Modified Pierson-Moskowitz spectra, and the heave motion of the vessel described by a time-series generated from the wave spectrum and the vessel response amplitude operators. Simulations showed that heave motion attenuation above 86% are possible without feedback from the tension in the cable. With cable tension feedback the figure was increased to 98%.

7.2 Suggestions for further work

This thesis has examined the mathematical modeling of a hydraulic heave compensator, cable and load. Further development of the model should include the dynamics of the winch and the crane (or A-frame), as well as incorporate the pump motor dynamics.

The placement of the lifting point on the vessel should be taken into consideration. If it is not exactly at the center of gravity of the vessel, then the roll and pitch will affect the heave motion. With an A-frame configuration, the lifting point is in the stern of the vessel and the pitch will be important. Likewise, the roll motion will influence the heave at the lifting point if the crane is positioned over the rail. A study of control for wave-load synchronization could also be appropriate.

Use of electrical heave compensators are becoming more widespread, and

a more thorough investigation of these systems and a comparison could be of interest. It could also be worth looking into the topic of regenerative techniques.

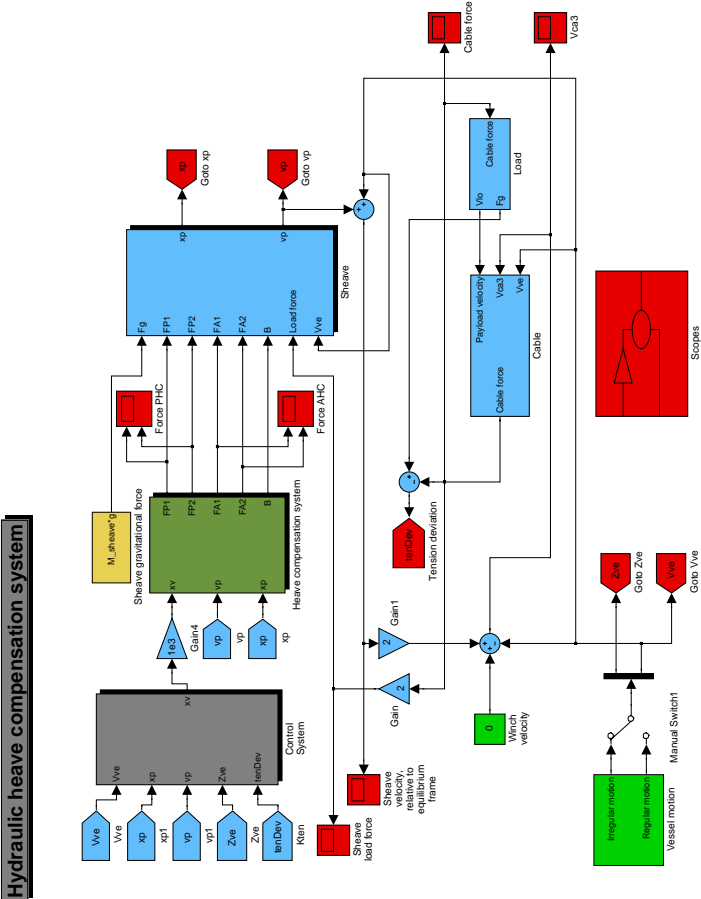
Bibliography

- Adamson, J. E. (2003). Efficient heave motion compensation for cable-suspended systems. In: *Underwater Intervention 2003*. New Orleans, LA, USA.
- Brautaset, K. (1983). *Innføring i oljehydraulikk*. Universitetsforlaget.
- Costain, B. M. and S. Bull (2006). Fiber ropes deemed viable for deepwater applications. *Offshore magazine*.
- Drevdal, K. E. (n.d.). Active heave drilling (tm), a new standard in heave compensation technology. Technical report. Hitec Drilling and Systems AS.
- Egeland, O. (1993). *Servoteknikk*. Tapir forlag.
- Egeland, O. and J. T. Gravdahl (2002). *Modeling and Simulation for Automatic Control*. Marine Cybernetics.
- Faltinsen, O. M. (1990). *Sea Loads on Ships and Offshore Structures*. Cambridge University Press.
- Fathi, D. (2004). Shipx vessel responses (veres). Technical report. Marintek AS Trondheim.
- Fossen, T. I. (2002). *Marine Control Systems: Guidance, Navigation and Control of Ships, Rigs and Underwater Vehicles*. Marine Cybernetics.
- Frumau, C. and W. Woldering (2007). Heave compensation system for deepwater installation. In: *Marine Construction Europe (MCE) Deepwater Development 2007*.
- GustoMSC (n.d.). Modular active heave compensation system for winch applications. Product sheet.
- ISSC (1964). In: *Proceedings of the 2nd International Ship Structures Congress*. Delft, The Netherlands.
- Kjølle, A. (1995). *Oljehydraulikk*. Tapir Forlag.

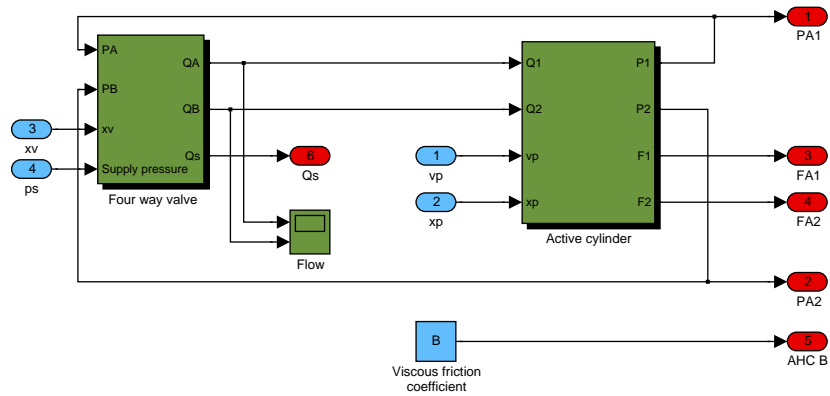
- Offshore (1999). Active heave drilling drawworks system goes to work. *Offshore magazine*.
- Pedersen, E. and H. Engja (2003). Mathematical modeling and simulation of physical systems. Lecture Notes in TMR4275 Modeling, Simulation and Analysis of Dynamic Systems, Department of Marine Technology, Norwegian University of Science and Technology.
- Penton Media, Inc. & Hydraulics & Pneumatics magazine (n.d.). <http://www.hydraulicspneumatics.com/>. Last accessed: 18.05.2007.
- Perez, T. (2005a). *Ship Motion Control: Course Keeping and Roll Stabilisation using Rudders and Fins*. Springer.
- Perez, T. and Ø. Lande (2006). A frequency-domain approach to modeling and identification of the force to motion vessel response. Technical report. Centre for Ships and Ocean Structures (CeSOS).
- Perez, T. and P. Steinmann (2007). Modelling and performance of an active heave compensator for offshore operations. In: *IFAC Conference on Control Applications in Marine Systems (CAMS)*.
- Perez, Tristan (2005b). A review of geometrical aspects of ship motion in manoeuvring and seakeeping, and the use of a consistent notation. Technical report. Marine System Simulator (MSS) Group, CeSOS, NTNU.
- Rosenberg, R. C. and D. C. Karnopp (1983). *Introduction to Physical System Dynamics*. McGraw-Hill Series in Mechanical Engineering. McGraw-Hill, Inc.
- Samantaray, A. K. (2005). About bond graphs. <http://www.bondgraph.info/about.html>.
- Skaare, B. (2004). Control of loads through the wave zone in marine operations. PhD thesis. Department of Engineering Cybernetics, Norwegian University of Science and Technology.
- Swail, V. R., V. J. Cardone, M. Ferguson, D. J. Gummer, E. L. Harris, E. A. Orelup and A. T. Cox (2006). The msc50 wind and wave reanalysis. In: *9th International Workshop On Wave Hindcasting and Forecasting*. Canada.

Appendix A

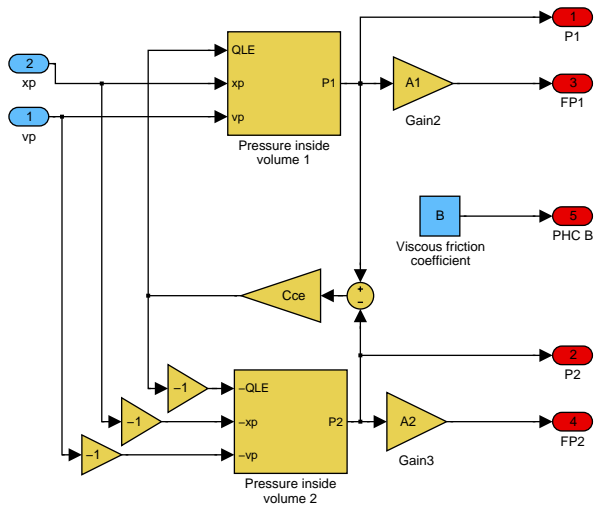
Simulink diagrams



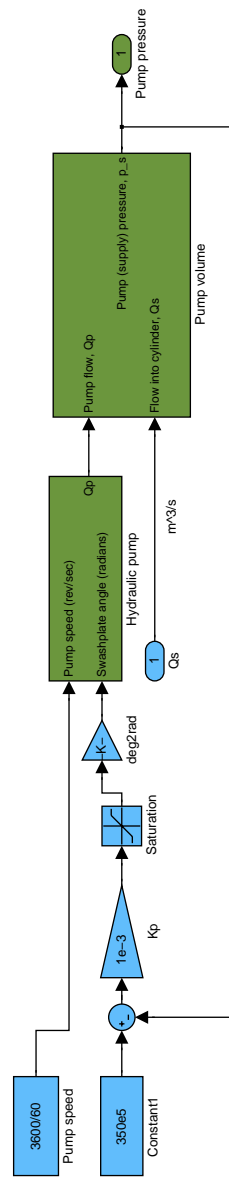
AHC subsystem



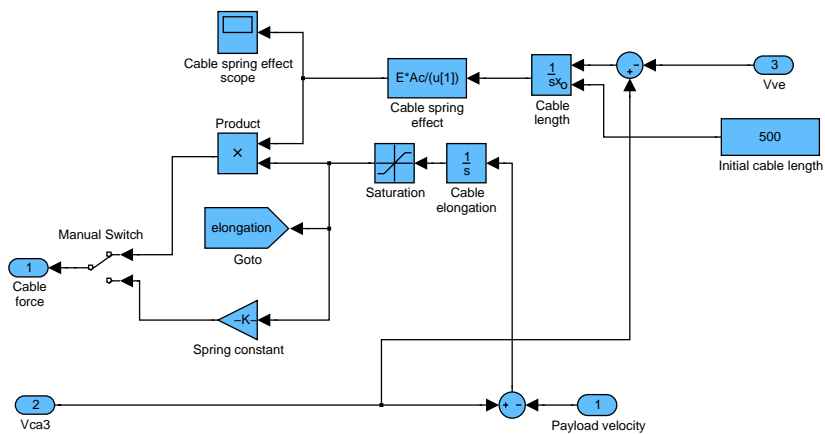
PHC subsystem



Inline piston pump



Cable



Load

